CHAPTER 3

Biophysical Methods to Study Tight Junction Permeability

Dorothee Günzel, Susanne M. Krug, Rita Rosenthal, and Michael Fromm
Institute of Clinical Physiology, Campus Benjamin Franklin,
Charité, Berlin, Germany

Current Topics in Membranes, Volume 65
1063-5823/10 $35.00

DOI: 10.1016/S1063-5823(10)65003-X

I. OVERVIEW

Transepithelial resistance (TER) can be determined, as a repetitive screening method, by chopstick electrodes directly on cell culture filters or, as a more reliable technique, in Ussing chambers. Although TER often serves as a rough indicator of tight junction permeability, only more advanced biophysical methods like impedance spectroscopy and conductance scanning allow to quantify changes in paracellular resistance and to separate these changes from those occurring in transcellular or subcellular resistance. These techniques are thus superior to conventional TER measurements which provide combined effects only. In addition, tight junction permeabilities can be determined by flux or diffusion potential measurements. It has to be kept in mind, however, that there is not one single permeability of a specimen, but that permeabilities are different for every ion or uncharged molecule of distinct size, as exemplarily shown for tricellulin which differentially modulates bicellular and tricellular tight junction permeabilities for ions and macromolecules. Paracellular permeabilities to water can be determined by transepithelial measurements on claudin-perturbed cells, as has been done for claudin-2 and claudin-10b. Finally, biophysical measurements provide information about tight junction channel properties such as pore size ion charge preferences, and may help to identify independent and parallel pathways.

II. INTRODUCTION

More than half a century ago, the terms "zonula occludens" and "tight junction" (TJ) were introduced after it had been shown in electron microscopic studies that these intercellular structures form a border against the passage of solutes across epithelia (Farquhar & Palade, 1963). Morphological differences were found between TJs of "leaky" and "tight" epithelia (Claude & Goodenough, 1973). The observation that sealing is dependent on the amount of horizontally oriented strands (Claude, 1978) is in line with the idea that this structure generally seals the paracellular space but in a more or less perfect way.

During the 1990s, only shortly after the discovery of the claudins, it turned out that many members of this protein family, such as claudin-1 and claudin-5, indeed seal the TJ, but there are also exceptions that behave differently, for example, claudin-2. Claudin-2 causes TJ strands to become leaky (Furuse, Furuse, Sasaki, & Tsukita, 2001) by forming paracellular cation-selective ion channels (Amasheh et al., 2002). This and similar findings of other channel-forming claudins restimulated research on permeability properties of the TJ with special focus on the understanding of specific barrier function and of mechanisms concerning disturbed barrier in epithelial and endothelial

diseases. Disturbed tight junctional barrier may have two functional consequences, (i) unwanted absorption of potentially harmful large solutes or (ii) excessive secretion of ions, followed by an osmotically equivalent amount of water which, in intestines, causes leak flux diarrhea.

Four points may be stressed regarding permeability studies of TJs:

First, conventional TER (transepithelial resistance) measurements do not adequately describe the resistance provided by the TJ. Perturbations of the TJ regularly cause a much larger change in paracellular resistance than is reflected in TER changes. Perturbations or pathologies may not only alter the paracellular but also the transcellular barrier, that is, cell membrane ion channels.

Second, in simple resistance measurements on native tissues like intestinal epithelia, adhering subepithelial layers add to total resistance. For inflammatory diseases, it is typical that subepithelial layers proliferate and thus increase in resistance while epithelial resistance decreases due to a TJ barrier defect. In the worst case, both changes compensate each other, resulting in an unchanged total resistance as detected by TER measurement.

Third, simply to state "the permeability" of a barrier is not a meaningful statement. In contrast to resistance, permeability always refers to a substance. This can be anything between small ions and macromolecules. However, frequently only one tracer is measured to determine "the permeability." Two opposing examples may illustrate that this is insufficient: Claudin-2-dominated TJs are permeable to small cations and water but not to anions or larger solutes (Amasheh et al., 2002; Rosenthal et al., 2010). In contrast, tricellulin-a abolishes the permeability of tricellular TJs to macromolecules but not to ions (Krug et al., 2009). Thus, at least the permeability to several solutes of different sizes should be determined in order to obtain a permeability profile of a barrier.

Fourth, permeabilities should be given as such (common unit: cm/s), not as marker flux rates or even concentration changes within the bathing fluid, because flux rates or concentration changes do not allow comparisons of results from different studies or for different markers.

In the following paragraphs, we describe strategies and methods allowing a detailed description of TJ resistance and permeabilities to various solutes and to water.

III. RESISTANCE MEASUREMENTS

A. Transepithelial Resistance (TER, R^t)

The most common measure of TJ permeability to ions is the "transepithelial electrical resistance" (TER or, in the symbolic language of electrophysiology, R^t). To be exact, R^t represents the reciprocal of the sum of the

permeabilities of all ions of the adjacent bath solution times their respective concentrations. In a simplified form, including only Na^+ and Cl^-, this relation is detailed in Eqs. (3) and (4).

In effect, in a nonselective epithelium, R^t mainly represents the permeabilities to Na^+, Cl^-, K^+ and, if present, HCO_3^-. The reciprocal of R^t is G^t, the transepithelial conductance, given in mS/cm^2 of gross epithelial area. It is clear that conductance is proportional to area, and consequently that resistance decreases with increasing area. This is the reason why R^t is expressed as Ω cm^2, not Ω/cm^2. In general, R^t is measured by applying a current pulse, ΔI, across the cell layer and recording the resulting voltage change ΔV. According to Ohm's law, the resistance is calculated as the voltage difference between both electrodes divided by the amplitude of the current pulse ($\Delta V/\Delta I$). Since any resistor located between the voltage-sensing electrodes is included in this raw resistance measurement, the contribution of the bathing fluid has to be determined without epithelium and then subtracted in order to obtain R^t.

B. Chopstick Electrodes

In confluent cell cultures grown on permeable filter supports, R^t can be conveniently and repetitively measured by commercially available "chopstick electrode" systems. However, chopstick measurements often yield values different from those obtained in standard Ussing-type chambers. There are several reasons for this discrepancy.

First, due to a nonuniform current field produced by the chopstick electrodes across the filter insert, R^t results may differ depending on the position of the electrode above the cell layer (Jovov, Wills, & Lewis, 1991). Especially in low-resistance cells, the access resistance from the lower side of the filter causes current to pass the filter mainly near its edge and, to a lesser degree, at the center of the filter. This effect is dramatically worsened in setups where the cells grow directly on metal electrode plates. It is clear from this that the electrodes should be positioned over the cell monolayers in a standardized way, for example, by a motorized adjusting apparatus.

A second disadvantage of the chopstick systems arises if solute net fluxes occur. Because the bathing fluids are static, unstirred layers develop and cause different concentrations of the transported solute on the apical and the basolateral side, which in turn affect flux rates and apparent permeabilities.

Furthermore, chopstick systems are usually driven by alternating clamp currents (AC) which, in part, short-circuit the ohmic-resistor elements of the cell layer. This causes a systematic underestimation of the true R^t proportional to both frequency and R^t.

Finally, chopstick systems without temperature control do not allow prolonged measurements because metabolic energy-driven transport and hence epithelial resistance is strongly temperature-dependent.

In conclusion, "chopstick" systems have to be used with caution, although they are good tools for screening the state of confluence of cell cultures, because they make repetitive measurements of identical filters possible.

C. Ussing Chamber

A reliable way to measure R^t is by means of four-electrode chambers, which are named after their inventor Hans Ussing (Ussing, 1949). Here, an almost homogenously distributed electric current (or DC current step; ΔI) is generated by two electrodes which are positioned at a distance from the epithelium (Fig. 1). This current is applied on the whole area of the epithelial layer and results in a voltage change (ΔV) that is sensed by two further electrodes close to the epithelium. The fluids on both sides of the epithelium are permanently stirred and temperature-controlled by a circulating bubble lift, which, at the same time, provides equilibration of these fluids with O_2 and CO_2, thus making experiments of several hours duration possible. Ussing chamber techniques, including the short-circuit technique for measuring active transport, are explained in detail, for example, by Clarke (2009) and Brown and O'Grady (2008).

D. Impedance Spectroscopy

In an attempt to investigate the specific function of single TJ proteins, simple R^t measurements on cell layers transfected with such proteins may give first crude indications, whether these proteins tighten the paracellular barrier, such as claudin-1 (Furuse et al., 2002) or claudin-5 (Amasheh et al., 2005; Nitta et al., 2003), or whether they increase paracellular ion permeability, as, for example, claudin-2 (Amasheh et al., 2002) or claudin-10 (Günzel, Stuiver, et al., 2009; Van Itallie et al., 2006).

However, R^t measurements are only of limited use to quantify these effects, as they do not discriminate between different resistance components of an epithelium. As illustrated in Fig. 2B, R^t consists of three major components. Two of them lie in parallel, the transcellular resistance (R^{trans}, dominated by the resistances of the basolateral and apical plasma membrane) and the paracellular resistance (R^{para}) which is formed by the TJ. A third resistor, the subepithelial resistance (R^{sub}), lies in series to R^{trans} and R^{para} and represents all resistances built by nonepithelial tissues or areas underneath the epithelia. In cell culture systems, it is present due to the filter support on which the cells are grown.

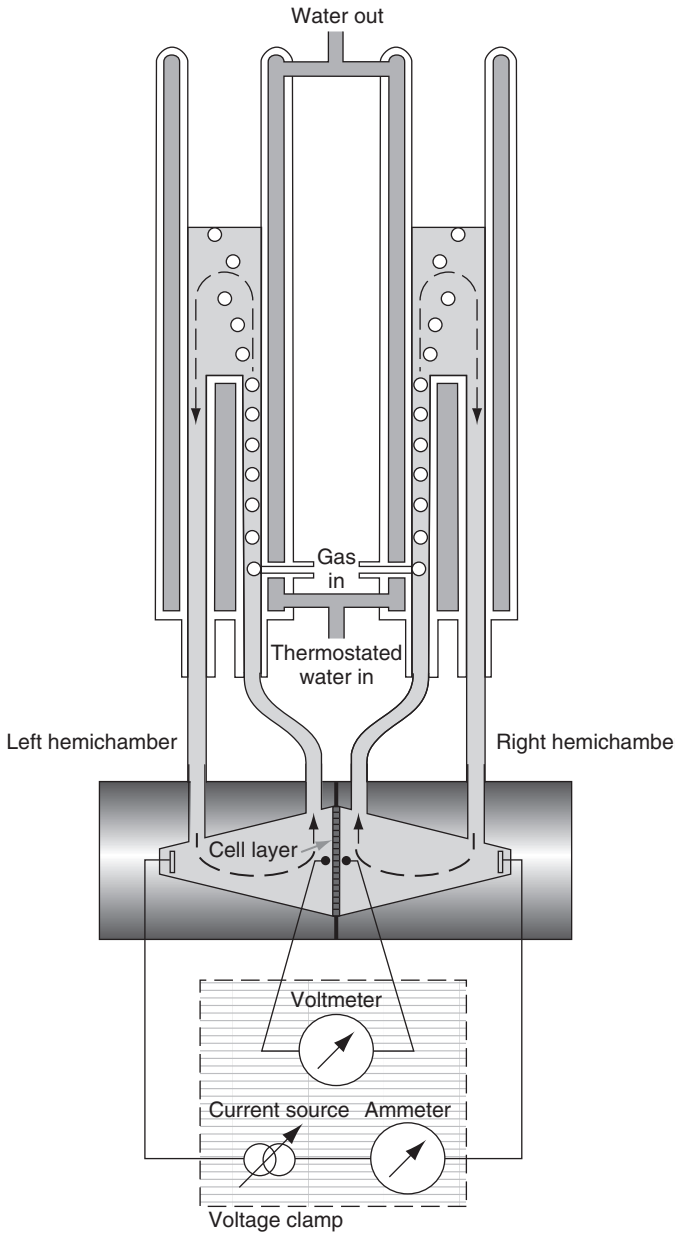

FIGURE 1 Schematic of an Ussing chamber. The chamber is named after the Danish physiologist Hans Ussing (1911–2000) and consists of two fluid-filled hemi-chambers which are separated by a filter-grown cell culture monolayer or a native epithelium. Two fluid reservoirs with gas lifts provide recirculation, gassing, and tempering of the bathing fluids. Driven by a voltage clamp unit, current is applied via two distant electrodes and voltage is sensed by two electrodes positioned close to the cell layer.

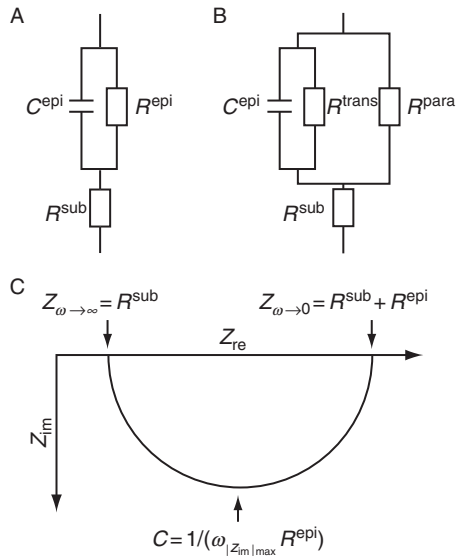

FIGURE 2 Equivalent electrical circuit of epithelia: (A) "One path impedance" measurements are based on an electrical model that only discriminates between subepithelial (R^{sub}) and epithelial (R^{epi}) resistance, and the epithelial capacity C^{epi}. (B) "Two-path impedance" measurements are based on the assumption that the epithelial resistance R^{epi} is composed of two resistances lying in parallel: a paracellular ($R = {}^{para}$) and a transcellular (R^{trans}) resistance. Under DC conditions or AC conditions at very low frequencies R^{epi} equals $R^{para} \times R^{trans}/(R^{para} + R^{trans})$. (C) Nyquist diagram (plot of the real and the imaginary portion of the impedance, Z_{re}, Z_{im}) for models shown in (A) and (B). For impedance values measured at different AC frequencies (angular frequency, ω), both models result in a semicircle. For high frequencies ($\omega \to \infty$), Z_{re} approaches R^{sub}, and for low frequencies ($\omega \to 0$), Z_{re} approaches $R^{t} = R^{sub} + R^{epi}$. The capacitance C^{epi} can be calculated from the frequency at which $|Z_{im}|$ reaches a maximum ($C^{epi} = 1/(\omega_{|Z_{im}|max} \times R^{epi})$. Adapted from Krug, Fromm, & Günzel (2009).

Impedance measurements have been used for almost a century to investigate the membrane properties of living cells (Cole & Curtis, 1938a, 1938b, 1938c; Curtis & Cole, 1938; Fricke, 1925; Höber, 1910; McClendon, 1927; McClendon, 1936) and since the 1940s to investigate the properties of epithelia (Teorell, 1946). Over the past decades, a great variety of equivalent electrical circuits with varying degrees of complexity were used to model epithelial properties. Impedance measurements make use of the fact that cell membranes act like capacitors and that under AC conditions capacitive reactances are strongly dependent on the frequencies employed (typically up to 50 different frequencies in the range of about 0.1 Hz up to several 10,000 Hz).

The inadequacy of conventional R^t measurements to compare epithelia under control and diseased states, or to study the potential barrier effects of drugs or hormones, and the necessity to employ impedance spectroscopy are illustrated by the following two examples.

First, when investigating the epithelial barrier in colonic biopsies from patients with inflammatory bowel diseases, it was found that R^t remained almost unchanged, although these patients clearly suffered from diarrhea caused by barrier loss and although claudin expression patterns were greatly changed. Further investigations employing impedance spectroscopy uncovered that a substantial decrease in R^{para} indeed occurred but was masked by a concomitant increase in R^{sub} (Bürgel et al., 2002; Kroesen, Dullat, Schulzke, Fromm, & Buhr, 2008; Zeissig et al., 2007).

Second, the application of the hormone aldosterone to colon epithelium increases expression of the epithelial Na^+ channel ENaC and thus causes a reduction in R^{trans}. However, a recent study (Amasheh et al., 2009) demonstrated that at the same time claudin-8 expression increased. Impedance measurements proved that this resulted in a several-fold increase in R^{para}. Despite this strong tightening of the paracellular barrier, the overall effect on R^t was a decrease.

These examples show clearly that simple R^t measurements do not necessarily reflect the barrier properties (i.e., paracellular tightness or leakiness) of an epithelium and that impedance measurements are a potent technique to differentiate between transcellular, paracellular, and subcellular effects.

E. One-Path Impedance Spectroscopy

In the simplest "lumped" model (Fig. 2A), epithelia are represented by three parameters: a membrane capacitance, C, an epithelial resistance, R^{epi}, and a subepithelial resistance, R^{sub}. All three parameters can be determined directly from impedance spectra by the equations given in the legend to Fig. 2C. In this model, only one single pathway for the current across the epithelium is supposed to exist. Therefore, impedance measurements based on this model have recently been dubbed "one-path impedance spectroscopy" (1PI) (Fromm et al., 2009).

1PI measurements were successfully applied in investigations on various inflammatory bowel diseases to uncover barrier loss, which, in simple transepithelial resistance measurements, is masked by a simultaneous increase in subepithelial resistance (Bürgel et al., 2002; Kroesen et al., 2008; Zeissig et al., 2007). Under physiological conditions, the thickness of the subepithelium does not contribute toward the transepithelial tightness because blood capillaries make their way through this subepithelial tissue and lie in direct vicinity to the epithelium. Under all inflammatory conditions, the leakiness of the epithelium

was increased by an upregulation of pore-forming claudins (e.g., claudin-2) and a concomitant downregulation of barrier-forming claudins (e.g., claudin-3, -4, -5, or -8).

F. Two-Path Impedance Spectroscopy

In the model underlying two-path impedance spectroscopy (2PI, Fig. 2B), R^{epi} is represented by a transcellular (R^{trans}) and a paracellular (R^{para}) fraction, that is, the current is assumed to cross the epithelium along two distinct pathways. To discriminate between these two pathways, additional measurements are necessary, as the equation system derived from impedance measurements is underdetermined (legend of Fig. 2B, for details, see Krug, Fromm, & Günzel, 2009).

In order to determine all four parameters (C, R^{sub}, R^{trans}, and R^{para}), studies from the 1980s employed intracellular impedance measurements using glass microelectrodes to gain information on the resistance and capacitance of the apical and basolateral plasma membrane (Kottra & Frömter, 1984). In an alternative approach, several studies used the high-resolution conductance scanning technique described later to analyze paracellular versus cellular resistances (Frömter & Diamond, 1972; Gitter, Bertog, Schulzke, & Fromm, 1997) and thus obtain sufficient information to solve the 2PI equation. As pointed out in the next section, conductance scanning is technically challenging, especially when used at its highest resolution and therefore not useful as a routine tool. A further approach to derive sufficient information to define all parameters within the epithelial equivalent circuit was a permeabilization of the plasma membrane by the application of ionophores (Clausen, Lewis, & Diamond, 1979; Lewis, Eaton, Clausen, & Diamond, 1977; Wills, Lewis, & Eaton, 1979).

In recent studies from our own lab, we used a combination of impedance spectroscopy and flux measurements of paracellular marker substances (e.g., fluorescein) while modulating the paracellular pathway, for example, by the removal of extracellular Ca^{2+} (Krug, Fromm, & Günzel, 2009; Reiter et al., 2006). The method is based on three assumptions: First, the reduction in the free extracellular Ca^{2+} concentration, induced by an application of EGTA, reduces the paracellular resistance without affecting the transcellular resistance (Ca^{2+} switch); second, fluorescein is a true paracellular marker, that is, it is exclusively transported along the paracellular pathway, and the resulting flux is proportional to the paracellular conductance (G^{para}); and third, the subepithelium does not affect fluorescein flux. If these assumptions are valid, then the following equation is valid:

$$G^{epi} = G^{trans} + G^{para} = G^{trans} + (s \times \text{fluorescein flux}) \quad (1)$$

with s being a constant; G^{epi}, epithelial conductance; G^{trans}, transcellular conductance; and G^{para}, paracellular conductance.

This is a linear equation. Plotting fluorescein flux values (x-axis) against G^{epi} values (y-axis) obtained from experiments during which only the paracellular pathway was modulated, should therefore result in a straight line with a y-intercept equaling G^{trans}.

As R^{sub}, G^{epi} ($=1/R^{epi}$), and C can be directly obtained from the impedance data and G^{trans} ($=1/R^{trans}$) and G^{para} ($=1/R^{para}$) can be determined from Eq. (1), the combination of EGTA switch experiments with a concomitant flux and impedance measurement allows a full description of all four epithelial parameters C, R^{sub}, R^{trans}, and R^{para} (Krug, Fromm, & Günzel, 2009). Applicability of this method could be confirmed in several cell lines such as the human colonic carcinoma cell line HT-29/B6 or the canine kidney cell line MDCK with its various subtypes (MDCK I, MDCK II, MDCK C7, and MDCK C11). It cannot be used on the human colonic carcinoma cell line Caco-2, as in these cells, fluorescein appears to be at least partially transported along the transcellular route.

Despite its being developed only recently, the 2PI spectroscopy technique has already been successfully employed in several studies to differentiate para- from transcellular effects on R^t (Amasheh et al., 2009; Krug et al., 2009; Krug, Fromm, & Günzel, 2009; Mankertz et al., 2009).

1. Example: Tricellulin and Tricellular Tight Junction

Tricellulin, a TJ protein discovered in 2005 (Ikenouchi et al., 2005) and predominantly localized in the tricellular meeting points of TJs, the tricellular TJ (tTJ), was assumed to be a barrier-forming and -stabilizing TJ protein. In overexpression studies in MDCK II cells, two types of clones were used. One differed solely in tricellular localization of tricellulin, the other differed in bicellular as well as tricellular localization. In this latter type, an increase in R^t was observed, which lacked in clones with overexpression restricted to the tTJ (Krug et al., 2009). 2PI spectroscopy disclosed that the threefold rise in R^{epi} in the bi- and tricellularly overexpressing clone was due to a 14-fold increase in R^{para}, while R^{trans} remained unchanged (Fig. 3). Although 2PI spectroscopy allows high resolution of even small changes in R^{epi}, there was no increase detectable in any of the three resistance parameters of the tricellularly overexpressing clone, indicating that the tricellular central tube has no measurable influence on R^t. Calculations using estimations of upper and lower limits of conductance underlined this finding, as in MDCK II cells the contribution of the tTJ on R^{epi} would only be $\sim 1\%$ of the contribution of the bTJ.

2. Example: Claudin-10b

As recently published, MDCK C7 cells transfected with claudin-10b exhibit a strong paracellular cation permeability that leads to a reduction in R^{epi} (Günzel, Stuiver, et al., 2009). Performance of 2PI spectroscopy seemed to be

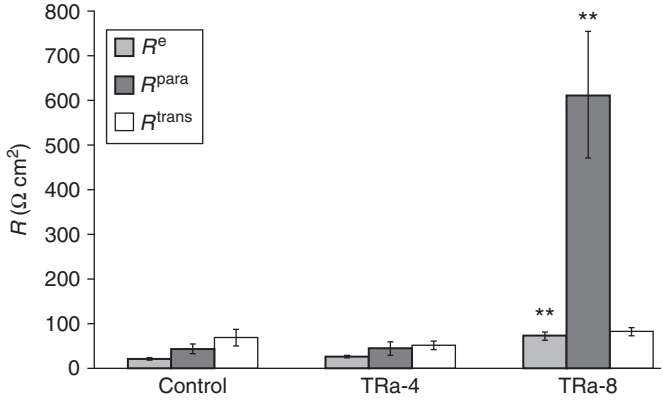

FIGURE 3 Two-path impedance spectroscopy of clones overexpressing TRIC-a. Tricellular overexpression of TRIC-a in TRa-4 cells did not change epithelial resistance (R^{epi}) in comparison to controls, while the bicellular overexpression of TRIC-a in TRa-8 cells induced a threefold increase in R^{e} (**$p < 0.01$; $n = 6$, 7, and 6, respectively). This increase was caused by a 14-fold rise of paracellular resistance (R^{para}, **$p < 0.01$), which is determined by the ion permeability of the TJ. Transcellular resistance (R^{trans}) was not significantly changed. From Krug et al. (2009).

suitable to analyze these findings employing fluorescein, Cl^-, and Na^+ as paracellular flux markers (Krug, Fromm, & Günzel, 2009). Plotting G^{epi} against the permeabilities of those flux markers yielded linear relationships. Extrapolation of the *y*-intercept for all three flux markers resulted in the same G^{trans}, while the slopes of the three relationships differed remarkably (Fig. 4). The slope of G^{epi}/Na^+ permeability was reduced to less than a half compared to G^{epi}/Cl^- permeability, indicating an increased P_{Na}/P_{Cl} as it was already observed by dilution potential measurements (Günzel, Stuiver, et al., 2009).

3. Example: Tumor Necrosis Factor-α and Claudin-2

Tumor necrosis factor-α (TNFα) is a proinflammatory cytokine which is elevated, for example, in active Crohn's disease. After the application of TNFα to HT-29/B6 cells, the performance of 2PI spectroscopy indicated a distinct decrease in R^{epi} which was solely due to a decrease in R^{para}, while the transcellular resistance R^{trans} remained unchanged (Mankertz et al., 2009; Fig. 5). Further examinations revealed an increased expression of claudin-2 after TNFα application to be responsible for the decrease of R^{para}. This claudin is also often upregulated in chronic intestinal inflammation such as Crohn's disease (Zeissig et al., 2007), supporting the finding that there is an influence of TNFα on tight junctional barrier function.

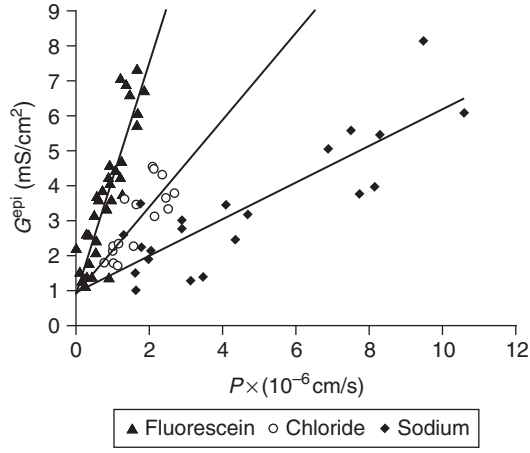

FIGURE 4 Plot of G^{epi} versus permeabilities for fluorescein, Cl^-, and Na^+ in clones expressing claudin-10b. Plotting of G^{epi} versus fluorescein (▲), Cl^- (○), and Na^+ (◆) permeability yields G^{trans} values of 0.94, 0.93, and 0.98 mS/cm^2, respectively, which have to be corrected by 0.6 mS/cm^2 for values in the absence of EGTA. R^{trans} thus amounts to 2860 Ω cm^2. The slope of G^{epi} versus Na^+ (0.50×10^3 S × s/cm^3) is lower than for Cl^- (1.12×10^3 S × s/cm^3) and fluorescein (3.3×10^3 S × s/cm^3), mirroring the claudin-10b-induced increase in cation permeability. From Krug, Fromm, & Günzel (2009).

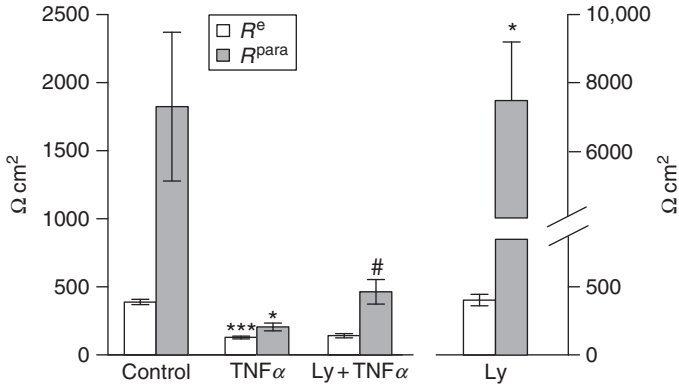

FIGURE 5 Two-path impedance spectroscopy of HT-29/B6 cells treated with TNFα. TNFα reduces the epithelial as well as the paracellular resistance. The effect can be attenuated by LY294002 (Ly) (R^{epi}, epithelial resistance; R^{para}, paracellular resistance). $*p < 0.05$, $***p < 0.001$, $\#p < 0.05$. From Mankertz et al. (2009).

G. Conductance Scanning

Conductance scanning (also named voltage scanning) techniques are methods based on the analysis of local differences in current density, recorded in the supraepithelial bath solution by glass microelectrodes during the application of a transepithelial clamp current. Since the inhomogeneous conductivity of an epithelium is evaluated, these methods allow to determine the size and distribution of local conductivities in the plane of flat epithelia. Thus, differentiation between para- and transcellular conductivities is also possible.

The general principle of the conductance scanning technique was pioneered by Frömter, who applied large direct currents and detected voltage peaks above TJs (Frömter, 1972; Frömter & Diamond, 1972). For our variant of the technique, we combined the high spatial resolution of a scanning glass microelectrode, as used by Frömter (1972), Hudspeth (1975), and Cereijido, Stefani, and Palomo (1980), with the superior signal-to-noise ratio of the lock-in principle (Foskett & Scheffey, 1989; Jaffe & Nuccitelli, 1974).

The setup consists of a four-electrode setup in a horizontal chamber plus a pair of mobile-scanning microelectrodes (Fig. 6). Epithelia or confluent cultured cell monolayers are mounted and viewed through a 20× or 40×

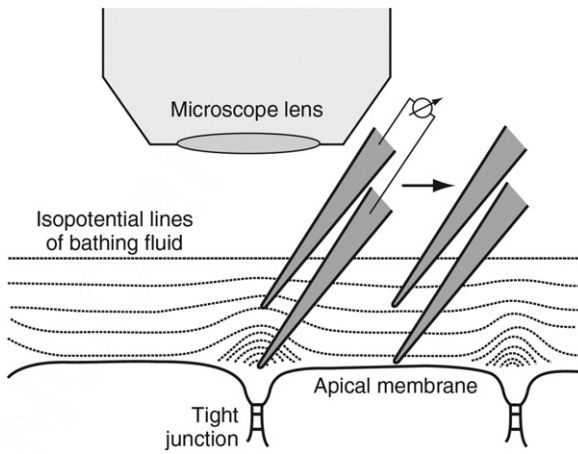

FIGURE 6 Principle of conductance scanning. An AC clamp current is applied across the cell monolayer and induces—depending on the resistances of the respective site—a major voltage drop across the cells and a very small one (μV range) across the bathing fluids, indicated by isopotential lines. The cell layer is scanned horizontally by a pair of jointed microelectrodes. The signal is detected by a phase-locked loop amplifier. Adapted from Fromm et al. (2009).

water-immersion objective lens. Alternating electric current of 0.2 mA/cm^2 and 24 Hz is clamped across the tissue and the electric field generated in the mucosal bath solution is measured with a pair of microcapillaries above the epithelial surface. In the present development, the two microcapillaries are glued together, yielding a tip distance of approximately 30–50 μm. The measured voltage between the tip openings varies in proportion to the local tissue conductance below the electrodes.

The position of the microelectrodes in relation to the tissue is adjusted by moving the experimental chamber with an electrically driven micromanipulator. The distance between the tissue and the lower scanning electrode is adjusted between 200 μm and virtually zero, depending on the intended spatial resolution. With the measured electric field and the known specific resistivity of the bath solution, the local current density is calculated. Together with the transepithelial voltage, this yields the local conductivity.

Depending on the distance between epithelium and scanning electrodes, different spatial resolutions are obtained. A list of applications, ordered with increasing resolution, include

- areas of ulceration (Gitter, Wullstein, Fromm, & Schulzke, 2001);
- colon surface epithelium versus crypt openings (Grotjohann et al., 1998; Köckerling & Fromm, 1993; Köckerling, Sorgenfrei, & Fromm, 1993);
- focal leaks as, for example, generated by bacteria (Troeger et al., 2007),
- single-cell wound repair (Florian, Schöneberg, Schulzke, Fromm, & Gitter, 2002; Günzel et al., 2006);
- leaks caused by epithelial apoptoses (Bojarski et al., 2001; Gitter, Bendfeldt, Schulzke, & Fromm, 2000a);
- paracellular versus transcellular pathway (Gitter, Bendfeldt, Schulzke, & Fromm, 2000b; Gitter et al., 1997; Schulzke et al., 2005).

A characteristic feature of the conductance scanning technique lies in the fact that it provides distinct local data. If conductance distribution of an epithelium is homogenous, this is no advantage, but in case of unequal, for example, focal, distributions, this technique is favorable over techniques which yield averaged data from the entire chamber opening.

At highest resolution, the resistance across the TJ, R^{para}, is determined. This requires the use of scanning electrodes with tip diameters of $\sim$1 μm and hence comparatively high resistances (resistance $\sim$4–5 MΩ when filled with 0.5 M KCl), and scanning very close (vertical distance $<$ 3 μm) to the surface of the cells (Gitter et al., 1997). Both requirements limit the applicability of the conductance scanning technique: Cell layers have to be very even and must not be covered with mucus in order to accurately position the scanning

electrodes so close above the cells. Furthermore, the high resistance of the scanning electrodes induces a high level of noise above which very small changes in potential have to be detected. For this reason, conductance scanning is only applicable if tight junctional conductance greatly differs from transcellular conductance.

Gitter et al. (1997) successfully used low-resistance MDCK C11 cell monolayers and found that the paracellular and transcellular pathways contributed approximately 80% and 20%, respectively, toward the total transepithelial conductance of $\sim$13 mS/cm^2 ($R^{epi} = 76\ \Omega\ cm^2$, $R^{para} = 95\ \Omega\ cm^2$, $R^{trans} = 385\ \Omega\ cm^2$). A later study on the same cell type (Amasheh et al., 2002) yielded similar values ($R^{epi} = 52\ \Omega\ cm^2$, $R^{para} = 68\ \Omega\ cm^2$, $R^{trans} = 221\ \Omega\ cm^2$). These values are somewhat higher than those recently obtained by 2PI spectroscopy ($R^{epi} = 41\ \Omega\ cm^2$, $R^{para} = 105\ \Omega\ cm^2$, $R^{trans} = 98\ \Omega\ cm^2$) and it yet needs to be established whether these differences are due to the different methods or whether they reflect natural variability in this cell type. Differences in R^{epi}, however, point toward the latter assumption, as in both cases, R^{epi} was measured using the same conventional Ussing chamber method described earlier.

In order to study the effects of claudin-2 transfected into high-resistance MDCK C7 cells, Amasheh et al. (2002) used a combination of impedance and conductance scanning techniques. In this study, they were able to demonstrate that the claudin-2-induced 3.6-fold reduction in R^{epi} was almost entirely due to a reduction in R^{para} from $\sim$2700 to 485 $\Omega\ cm^2$.

IV. ION PERMEABILITY MEASUREMENTS

Although conventional Ussing chamber experiments do not allow a direct discrimination of R^{trans} and R^{para}, they allow the analysis of ion selectivities and permeabilities of the paracellular pathway, and estimates of the paracellular pore size. These data have recently provided the basis for a modeling of the paracellular pore architecture (Yu et al., 2009).

Various methods have been established to determine epithelial ion permeabilities and three of these methods are briefly outlined in the following paragraphs. A major difficulty of all methods is finding a way to distinguish between the paracellular and transcellular pathways. Generally, it is assumed that paracellular ion movement is nonrectifying, that is, independent of the direction of measurement. If flux in the apical to basolateral direction differs from that in the opposite direction, it is usually assumed that the difference is due to transcellular ion transport. Ways to distinguish between paracellular and transcellular ion movements include pharmacological inhibition of the

transcellular route or carrying out the experiments at low temperature, as active ions transport mechanisms show a stronger temperature dependence than passive (diffusive) transport mechanism.

A. Ion Flux Measurements

Ion permeabilities can be measured directly if suitable radioactive isotopes are available. This is the case for Na^+ (^{22}Na, $t_{1/2} = 2.6$ years), Cl^- (^{36}Cl, $t_{1/2} = 3.0$ years), and Ca^{2+} (^{45}Ca, $t_{1/2} = 162.7$ days). ^3H- or ^{14}C-labeled organic ions may also be available. Difficulties arise with K^+ (^{40}K is not available, but sometimes ^{86}Rb is used as a surrogate; however, see below for differences in permeability) and with Mg^{2+}. ^{28}Mg ($t_{1/2} = 21$ days) is practically unavailable, ^{27}Mg ($t_{1/2} = 9.46$ min) is so short-lived that it is only of very limited use (however, see Bijvelds, Kolar, Wendelaar-Bonga, & Flik, 1996; Bijvelds, Kolar, Bonga, & Flik, 1997).

As a rule, a small (micromolar) amount of a radioactive tracer is added to the saline on the apical or basolateral side (=donor side) and aliquots are collected from the other side (=acceptor side) at regular intervals to determine flux as the transported amount per time and epithelial area. Flux data can easily be converted into permeabilities by multiplication with the concentration of the investigated ion in the saline.

Flux measurements are usually carried out under equilibrium exchange conditions, that is, the stable isotope or unlabeled organic ion is present in the saline at physiological (millimolar) concentrations on both sides of the cell layer. These unidirectional flux measurements have the advantage that they are carried out under equilibrium conditions and thus reflect the physiological situation.

If no radioactive isotope or labeled compound is available, flux measurements can be carried out under "zero-trans" conditions, that is, the acceptor side initially does not contain the ion under investigation and its accumulation is detected by an appropriate analytical technique (ion-selective electrode, colorimetric reaction, atomic absorption spectrometry, HPLC, etc.). Results obtained under zero-trans conditions may differ from those obtained under equilibrium exchange conditions, as transport kinetics under both conditions are different. Furthermore, TJ properties may be directly affected by the ion gradient used under zero-trans conditions. For example, withdrawal of Ca^{2+} from one side of the epithelium in order to measure Ca^{2+} flux may cause a loss of TJ barrier function (Martinez-Palomo, Meza, Beaty, & Cereijido, 1980). Application of a pH-gradient to determine paracellular H^+ transport has been applied successfully (Angelow, Kim, & Yu, 2006);

however, it has to be kept in mind that changes in extracellular pH may titrate charged side-chains within the tight junctional pore and thus cause a loss of pore selectivity.

B. Dilution and Biionic Potentials

Ion selectivities of epithelia can be estimated from diffusion potentials that build up across these epithelia if ion gradients are applied. To determine, for example, if Na^+ and Cl^- permeabilities (P_{Na}, P_{Cl}) of an epithelial barrier differ, part of the NaCl in the bath solution on one side of the epithelium is replaced iso-osmotically by an uncharged substance, for example, mannitol. Thus, NaCl is "diluted" on one side of the epithelium. If $P_{Na} \neq P_{Cl}$, a transepithelial potential difference (dilution potential, ΔE) will develop which, for $P_{Na} > P_{Cl}$, is positive on the diluted side relative to the unchanged side, while it is negative for $P_{Na} < P_{Cl}$. Ideally, P_{Na}/P_{Cl} can be calculated using the Eq. (2).

$$\frac{P_{Na}}{P_{Cl}} = \frac{10^{(\Delta E/s)} \cdot a_{Cl}^{ap} - a_{Cl}^{bl}}{a_{Na}^{ap} - 10^{(\Delta E/s)} \cdot a_{Na}^{bl}} \quad \text{with } \Delta E = E_{bl} - E_{ap}; \quad s = 2.303(RT/F) \tag{2}$$

a_{ion}^{ap}, a_{ion}^{bl} apical and basolateral ion activities; R, universal gas constant; T, absolute temperature; F, Faraday constant.

Absolute permeabilities can be calculated from P_{Na}/P_{Cl} and the epithelial conductance using the following two equations (Eqs. (3) and (4), see Hou, Paul, & Goodenough, 2005):

$$P_{Cl} = \frac{G}{[NaCl]} \frac{RT}{F^2} \frac{1}{(1 + P_{Na}/P_{Cl})} \tag{3}$$

$$P_{Na} = P_{Cl} \frac{P_{Na}}{P_{Cl}} = \frac{G}{[NaCl]} \frac{RT}{F^2} \frac{1}{1 + (P_{Na}/P_{Cl})} \frac{P_{Na}}{P_{Cl}} \tag{4}$$

where G, transepithelial conductance (1/(transepithelial resistance)); [NaCl], NaCl concentration.

Similarly, relative permeabilities of other monovalent cations can be determined by replacing part of the Na^+ on one side of the epithelium by the cation of interest (X^+) and measuring the resulting transepithelial potential ("biionic potential") and using Eq. (5).

$$\frac{P_X}{P_{Na}} = \frac{10^{(\Delta E/s)} a_{Na}^{bl} - a_{Na}^{ap}}{a_X^{ap} - 10^{(\Delta E/s)} a_X^{bl}} \tag{5}$$

However, Eq. (5) is only valid if $P_X \gg P_{Cl}$. If this is not the case, Cl^- will diffuse across the epithelium along the electrical gradient and thus dissipate at least part of the biionic potential. Therefore, in most cases, it is advisable to use Eq. (6) instead of Eq. (5), which takes into consideration the effects of Na^+, Cl^-, and the cation X^+:

$$\frac{P_X}{P_{Na}} = \frac{a_{Na}^{ap} + (P_{Cl}/P_{Na})a_{Cl}^{bl} - 10^{(\Delta E/s)}\left(a_{Na}^{bl} + (P_{Cl}/P_{Na})a_{Cl}^{ap}\right)}{10^{(\Delta E/s)}a_X^{bl} - a_X^{ap}a_{X-ap}} \tag{6}$$

The ratio P_{Cl}/P_{Na} within Eq. (6) has to be determined from separate dilution potential measurements, preferably from the same cell layer. Subsequently, absolute permeabilities can be calculated from P_{Na} values obtained from Eq. (4).

Although the general principle of these measurements is relatively simple, there are several pitfalls that have to be avoided to obtain correct permeability values.

First, active (transcellular), electrogenic transport may be activated by the solutions used to determine dilution/biionic potentials. Therefore, measurements should always be carried out in the apical to basolateral as well as in the basolateral to apical direction to determine whether the resulting potentials are symmetrical. If not, the pharmacological inhibition of active transport components may be considered. Alternatively, experiments may be carried out at lower temperatures in order to inhibit active transport.

Second, insufficient movement of the bath solution during the experiment may cause so-called "unstirred layer effects," that is, an enrichment/depletion of the transported ion in close vicinity to the cell membrane that will affect local ion gradients and thus the resulting potentials.

Third, Eqs. (2), (5), and (6) require the use of ion activities rather than concentrations. At physiological ion strengths, activity coefficients are clearly different from unity and therefore have to be taken into consideration. However, activity coefficients of complex solutions are difficult to estimate. Several approaches, such as the Debye–Hückel formalism, may be used for an approximation (for a detailed discussion, see e.g., Ammann, 1986; Barry, 2006; Sugiharto, Lewis, Moorhouse, Schofield, & Barry, 2008).

Fourth, liquid junction potentials (LJP) occur at the interface between the apical and basolateral solutions in the Ussing chamber and the salt bridges used to connect the bath to the voltage electrodes. As long as the apical and basolateral side of the chamber contain the same solution, LJPs on both sides should be of the same magnitude, but of opposite sign, and thus cancel each other out. As soon as the ion compositions on both sides differ, the LJPs will differ and the resulting potential difference will add to the diffusion potential

and distort the results. It is the "first law of electrophysiology" (Thomas, 1978) that 3 M KCl electrodes yield correct results as they minimize LJPs. However, agar bridges used in Ussing chambers usually have large diameters and therefore lose KCl to the surrounding solution, causing "history effects" (Barry & Diamond, 1970), that is, potentials that depend on the duration of exposure to different solutions. Alternatively, salt bridges may be used that contain NaCl concentrations close to those used during the experiments, to minimize leakage and then to measure or calculate the LJP that will occur, when the solution on one side of the chamber is changed. Again, this is not trivial. Often, measurements across blank filter membranes are used to measure the overall effect at the two salt bridges; however, a further LJP will develop at this membrane and render the result useless (see supplement to Yu et al., 2009 for a detailed discussion).

In summary, it is preferable to use 150 mM NaCl bridges and to calculate LJPs using the Henderson formalism instead of relying on salt bridges containing high KCl concentrations or attempting to measure LJP (Barry & Diamond, 1970; Ammann, 1986, supplement to Yu et al., 2009):

$$V_j = V_{sol} - V_{ref} = \frac{RT}{F} \frac{\sum_i \left(z_i u_i \left(a_i^{sol} - a_i^{ref}\right)\right)}{\sum_i \left(z_i^2 u_i \left(a_i^{sol} - a_i^{ref}\right)\right)} \ln \frac{\sum_i \left(z_i^2 u_i a_i^{ref}\right)}{\sum_i \left(z_i^2 u_i a_i^{sol}\right)} \qquad (7)$$

where V_j is the liquid junction potential between bath solution (sol) and reference or agar bridge (ref), respectively; u_i is the absolute mobility of ion i (tables: see e.g., Ammann, 1986; Barry & Lynch, 1991; Meier, Ammann, Morf, & Simon, 1980; Morf, 1981; Ng & Barry, 1995; Robinson & Stokes, 1959; Yu et al., 2009); a_i is the single ion activity of ion i within bath solution (sol) and reference or agar bridge (ref), respectively; z_i is the charge number of ion i; R is the universal gas constant; T is the absolute temperature; and F is the Faraday constant.

C. Conductance Measurements

Changes in conductance induced by changes in ionic composition of the bath solution have been interpreted in terms of differences in the permeabilities of the ions involved (Tang & Goodenough, 2003; Yu et al., 2009). For the interpretation of such data, it has to be kept in mind that part of the conductance measured is due to the transcellular pathway and that this pathway might also be affected by the imposed changes in ionic composition of the bath solution. Yu et al. (2009), therefore, only investigated differences in conductance in cells transfected with Tet-Off/claudin-2 in the presence and absence of doxycycline (Dox). Both Tang and Goodenough (2003) and

Yu et al. (2009) find that data obtained from conductance measurements do not necessarily match data obtained from flux or dilution potential measurements and conclude that all inorganic cations investigated compete for the same pore.

1. Implications: Channel Properties of Claudins

First indications that members of the claudin family may affect paracellular ion permeability were published about a decade ago (claudin-2, Furuse et al., 2001; claudin-4, Van Itallie, Rahner, & Anderson, 2001; claudin-16, Simon et al., 1999). Amasheh et al. (2002) further investigated claudin-2-induced changes in paracellular ion permeability using dilution potential and flux measurements, and found that claudin-2-overexpression in high-resistance MDCK C7 cells not only greatly decreased R^t but that this effect was specifically due to an increase in P_{Na}, while P_{Cl} remained constant. Amasheh et al. (2002) further demonstrated that the permeabilities of cations of various sizes (Na^+, K^+, $NMDG^+$, $choline^+$) were increased, while permeabilities to anions (Cl^-, Br^-) and uncharged molecules (mannitol, lactulose, and 4-kDa dextran) were unaffected. Claudin-2 thus behaved like a nonselective cation channel. Yu et al. (2009) showed in further investigations that upon the expression of claudin-2, the permeability sequence for alkali metal ions was $K^+ > Rb^+ > Na^+ > Li^+ \gg Cs^+$ and thus resembled Eisenman sequence V to VIII. The ratio between the permeabilities of the most permeable cation (K^+) and the least permeable (Cs^+) was 1.6, which is relatively narrow and suggests that the interaction sites within the pore are widely spaced (Eisenman, 1962) and/or partially hydrated (Yu et al., 2009). Permeability measurements for various organic ions of different sizes further indicated a pore diameter of approximately 6.5 Å at the narrowest point of the claudin-2 pore (Yu et al., 2009). Based on these data, Yu et al. (2009) performed Brownian dynamics simulation and obtained a pore model as best fit that assumed a channel length of 32 Å and funnel-like entrances of 16 Å in diameter, narrowing to 6.5 Å in diameter at the center of the pore. From this model, they were able to estimate single-channel conductance to be in the order of 100 pS.

Similar to claudin-2, the overexpression of mouse claudin-10b in MDCK C7 cells greatly increases cation permeability. However, in contrast to claudin-2, claudin-10b changed the permeability sequence to $Na^+ > Li^+ > K^+ > Rb^+ > Cs^+$, corresponding to Eisenman sequence X (Günzel, Stuiver, et al., 2009). In this study, P_{Na}/P_{Cs} was in the order of 3, indicating that the spacing of electric charges within the pore is narrower than in claudin-2 pores. This correlates well with the higher number of negative charges within the first

extracellular loop of claudin-10b (five negatively charged amino acids) compared to claudin-2 (three negatively charged amino acids, of which only one, D65, appears to reside within the pore, Yu et al., 2009).

In contrast to claudin-10b, the first extracellular loop of claudin-10a contains only one (human) or two (mouse) negatively charged, but seven positively charged amino acids. Overexpression of claudin-10a conveys an anion preference to the TJ, mainly through the arginine residues R33 and R62 (Van Itallie et al., 2006).

Claudin-16 had been assumed to form paracellular pores for divalent cations for two reasons: (i) claudin-16 mutations cause renal loss of Ca^{2+} and Mg^{2+} and (ii) claudin-16 is expressed in the thick ascending limb of Henle's loop which has previously been identified as the major location for (paracellular) Mg^{2+} absorption in the kidney. As recently reviewed by Günzel and Yu (2009), however, data from claudin-16 overexpression studies are conflicting. Ca^{2+} and Mg^{2+} permeabilities were measured using the various methods described earlier (equilibrium and zero-trans flux measurements, biionic potential measurements), but, if present at all, were only minor (Günzel, Amasheh, et al., 2009; Ikari et al., 2004; Kausalya et al., 2006; Hou et al., 2005). While Hou et al. (2005) found an increased Na^{+} permeability in transfected LLC-PK1 cells, Kausalya et al. (2006) and Günzel, Amasheh, et al. (2009) failed to do so in MDCK C7 cells. Thus, the role of claudin-16 as a pore-forming claudin yet remains unsolved.

V. FLUXES OF UNCHARGED PARACELLULAR TRACERS

Fluxes of different-sized hydrophilic tracers are often measured to determine paracellular permeability properties. To this end, radioactively labeled substances as urea, mannitol, inulin, or polyethylene glycols (PEGs; Ghandehari, Smith, Ellens, Yeh, & Kopecek, 1997) and/or fluorescence-labeled dextrans (Sanders, Madara, McGuirk, Gelman, & Colgan, 1995) have been used.

Passage through paracellular pores is a passive process and, as described earlier, flux measurements are usually carried out under equilibrium exchange conditions. It is therefore attempted to abolish gradients between donor and acceptor sides by adding equal amounts of the unlabeled species of the analyzed probe to the apical and basolateral bathing solution. Beforehand, however, probes such as dextrans or PEGs should be dialyzed. Although labeled with an average molecular weight, these molecules do not have a precisely defined size but contain a range of different sizes. In addition, these rather fragile probes may decay over time. Preferential permeation of the resulting smaller fragments would consequently distort the results and overestimates of paracellular pore sizes.

The fluxes (J) of the measured probes are then calculated by

$$J = \frac{\Delta c V_{ch}}{\Delta t A} \tag{8}$$

where Δc is the concentration difference of the probe in the acceptor chamber at time t_1 and t_2; Δt is the time difference $t_2 - t_1$; V_{ch} is the volume of hemi-chamber; and A is the area of the specimen.

Fluxes are expressed as nmol/h/cm^2 and give a first insight into the characteristics of paracellular pores formed by TJ proteins. However, due to the concentration dependence, fluxes from different studies cannot simply be compared. It is therefore preferable to convert fluxes into apparent permeabilities, P_{app}. The unit is formally that of a speed, but originates from the division of the flux by the concentration of the measured solute:

$$P_{app} = \frac{J}{c_{fin}} (10^{-6}\,\text{cm/s}) \; = (\mu\text{mol/h}/3.6/\text{cm}^2) \; / \; (\text{mmol/l}) \tag{9}$$

where J is the flux of the measured probe and c_{fin} is the concentration of the probe in the donor chamber.

Monitoring individual paracellular probes give rough estimations of the character of paracellular pores formed by TJ proteins.

First examinations using membrane-impermeant tracers suggested tight junctional pore diameters of ~6 Å (Spring, 1998), which is similar to some conventional ion channels (Balasubramanian, Lynch, & Barry, 1997; Goulding, Tibbs, Liu, & Siegelbaum, 1993).

Measurement of permeability for ethanolamine with a diameter of ~4.9 Å (Dwyer, Adams, & Hille, 1980) and for mannitol with ~7.2 Å (Madara & Dharmsathaphorn, 1985) refined the paracellular pore diameter to at least 4.9 Å, but not much bigger than 7 Å (Tang & Goodenough, 2003). Mannitol appeared not to move freely through the paracellular pore as it had been observed that there was a disproportionately larger permeability for compounds smaller than mannitol (Artursson, Ungell, & Lofroth, 1993; Knipp, Ho, Barsuhn, & Borchardt, 1997; Tang & Goodenough, 2003; Tavelin et al., 2003).

In 2001, an elegant technique measuring the permeabilities for 24 PEG sizes was developed simultaneously (Watson, Rowland, & Warhurst, 2001). Separation of the oligomers by liquid chromatography–mass spectrometry (LC–MS) allowed detailed functional profiling and mathematical modeling of the paracellular route. Profiling of fluxes across T84 and Caco-2 cells showed permeability to be biphasic, consisting of one size-restrictive, high-capacity pathway due to abundant, but small (diameter of ~8 Å) pores, and a low-capacity pathway which is size-independent and can be explained by sparse but much larger pores.

Profiling of the paracellular pathway employing a separation of modified PEGs by HPLC, where retention times are proportional to the molecular mass, showed that the pore aperture of ~8 Å in diameter was similar in all cell types

investigated (MDCK II cells, MDCK C7 cells, Caco-2 cells, and porcine ileum) although those cell types differ significantly in electrical resistance (Van Itallie et al., 2008; Fig. 7).

Comparison of P_{app} from PEG profiles allowed the estimation of relative pore numbers in various cell types. Expression of claudin-2 resulted in a selective increase in the number of small pores as the permeability for PEGs up to ~4 Å increases, while a knockdown of claudin-2 did not alter the number and size of these small pores (Van Itallie et al., 2008). From these findings, the permeability to small solutes was suggested to be proportional to the pore number and the profile of TJ proteins expressed, which would explain the dissociation between P_{app} for noncharged solutes and electrical resistance.

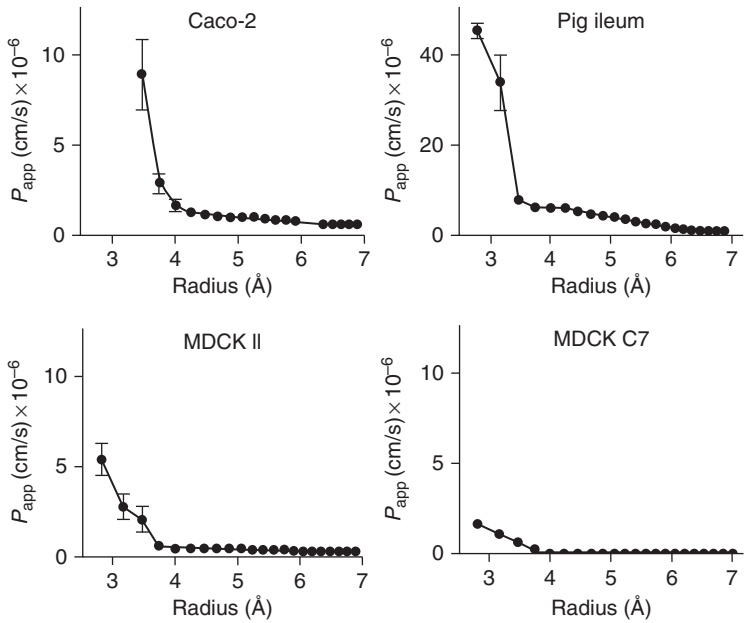

FIGURE 7 P_{app} as a function of PEG radius in Caco-2, MDCK II, and MDCK C7 monolayers and *ex vivo* pig ileum. All cell types show a size-restrictive pore calculated to be of radius ~4 Å. Ileum appears to have an additional pore cutoff at ~6.5 Å. In contrast to their similar pore size, the number of pores (reflected in the $P_{app} < 4$ Å) is highly variable. Caco-2 cells have the largest numbers of pores as well as the greatest permeation through the size-independent pathway; MDCK II cells have an intermediate number and MDCK C7 cells have few pores and little permeation through the second pathway. The relative pore number in pig ileum cannot be compared with that of cell lines because of the difference in the amplified surface area in intact tissue compared with the flat cultured cell monolayers. From Van Itallie et al. (2008).

Widely consistent with this model of two different pathways of passage, it was found that after the overexpression of tricellulin in tTJs of MDCK II cells, the permeability for macromolecules was remarkably decreased, while additional overexpression in bTJs led to increasing electrical resistance and decreasing permeabilities for ions (Krug et al., 2009). From these findings, different localizations of the two pathways were deduced. The high-capacity "small pores" were suggested to be an integral part of the bicellular junctions and thus frequent enough to carry ~99% of the paracellular permeability for ions, while the size-independent "large pores" were located at the tricellular central tube, which is wide enough to allow the passage of large solutes but rare enough to contribute only ~1% toward paracellular ion permeability.

VI. PARACELLULAR WATER TRANSPORT

Not only ions or macromolecules but also large volumes of water may be transported across epithelia not only through transcellular but also through paracellular routes (Rosenthal et al., 2010).

The transcellular route mediated by aquaporin water channels (Agre et al., 1993) is well described, but there is an ongoing dispute concerning the existence of significant water flow across the TJ (Spring, 1998). Although TJs are often named aqueous pores, there was yet no direct experimental evidence for a paracellular water flux because it is difficult to separate the TJ-controlled paracellular from transcellular water flux.

Technically, the obvious method for the determination of paracellular water flux would be to measure the rate of transepithelial water flux before and after blocking the TJ pathway. However, this approach has proven unsuccessful because the transcellular side effects of paracellular permeability inhibitors could not be excluded (Poler & Reuss, 1987). The converse procedure, blocking the transcellular water channels and measuring the resulting decrease in transepithelial water flux, is inapplicable since mercury, the only potent blocker of aquaporins, is not effective on all aquaporin isoforms (Knepper, 1994) and additionally, mercury applied in effective concentrations is cytotoxic in many cells and tissues.

Since suitable inhibitors of water movement across either pathway are not available, the permeability of the paracellular pathway has been determined indirectly by several methods. One method is to measure the water permeability of the apical and basolateral cell membrane and the transepithelial water permeability, and to calculate the paracellular water permeability from these data (Carpi-Medina & Whittembury, 1988; Flamion, Spring, & Abramow, 1995). The apical and basolateral cell membrane water permeability was

calculated from the rate of cell swelling or shrinkage after changing to an anisosmotic solution (apical or basolateral) in combination with the determination of the cell surface area, while an analysis of epithelial cell volume was performed with light microscopy. From a comparison of transepithelial and cell membrane water permeability, it was concluded that in rabbit renal proximal tubule, about 50% of the water passes through the paracellular pathway.

Another indirect approach involves the flux measurements of nonelectrolyte radiolabeled tracers across the epithelial layer for the estimation of paracellular water movement (Hernandez, Gonzalez, & Whittembury, 1995; Shachar-Hill & Hill, 1993; Steward, 1982; Whittembury, Malnic, Mello-Aires, & Amorena, 1988). As already discussed earlier, the fluxes of labeled tracers of definite size and molecular weight are also used for the evaluation of the TJ pore size. A precondition of this method is that the tracers cannot use the transcellular pathway and the assumption is that paracellular water movement induces a solvent drag of these paracellular probes (Spring, 1998). The net flux of these solutes is affected when the rate of the transepithelial volume flow is altered by changing the osmotic gradient across the epithelial layer. Thus, the flux data are used to calculate the fraction of water flow across the TJ. The fraction of paracellular water flow estimated by this method varies between 50% and 100% of the transepithelial flow.

Apart from these indirect measurements, optical microscopic approaches have been reported: One method used confocal microscopy in combination with fluid-phase fluorescent tracer technique for visualizing water secretion and differentiating the routes of water transport across epithelial layers (Segawa, Yamashina, & Murakami, 2002). In this approach, the acinar lumen of parotid and submandibular glands were perfused with fluorescent tracers and the intensity of the luminal fluorescence was observed before and after the stimulation of fluid secretion. Stimulation of fluid secretion caused a rapid decline of luminal fluorescence intensity, indicating that the secreted water washed out the fluorescent tracer in the luminal space. From the pattern of fluorescence decline under different experimental conditions, the authors conclude that water secretion occurs via the trans- and paracellular route.

Another optical microscopic technique was developed for a direct visualization of the fluid movement within the lateral intercellular spaces (LIS) of low-resistance MDCK cells, which represent a fluid-absorptive renal cell line (Kovbasnjuk, Leader, Weinstein, & Spring, 1998). Fluid movement within the LIS can be visualized by introducing a fluorescent dye which is trapped in the LIS and observing the concentration profile of this dye along the LIS. Since the flow velocity was near zero adjacent to the TJ and could not be augmented by the imposition of an osmotic gradient for the induction of transepithelial fluid movement, the authors conclude that a significant transjunctional flow does not occur.

As described earlier, approaches to distinguish between para- and transcellular water permeability are technically very difficult and these investigations yielded, in part, contrary results. None of these studies related the results to the molecular composition of the TJ.

1. Example: Claudin-2 and Paracellular Water Transport

In an alternative approach, the overall transepithelial water flux was measured before and after selective molecular perturbation of the TJ (Rosenthal et al., 2010). Chosen perturbators were claudin-2 and claudin-10b, both of which form cation channels when overexpressed in the TJ of MDCK C7 cells which lacks endogenous expression of these TJ proteins (Amasheh et al., 2002; Günzel, Stuiver, et al., 2009). Transepithelial water permeability was measured in a modified Ussing chamber with two separated silanized glass tubes instead of the gas lifts. Fluid movement was induced by an osmotic or ionic (Na^+) gradient and the fluid level in both tubes was monitored by a video-optic system at different times over a period of 2 h. The water flux was calculated (Fig. 8A) from the difference between the menisci at the registration times. The study revealed that water flux in claudin-2-transfected cells was elevated under all experimental conditions compared to control cells, whereas claudin-10b transfection did not alter water flux, although both claudins are permeable for small cations (Fig. 8B). In claudin-2-expressing cells, water flux could not only be induced by an osmotic gradient but also by a sodium flux through the TJ without any osmotic gradient. From these data, the authors conclude that claudin-2, but not claudin-10b, forms a paracellular water channel and by this mediates the paracellular part of water transport in leaky epithelia.

VII. EXPERIMENTAL STRATEGIES FOR TJ PERTURBATION

For perturbing the TJ experimentally, different approaches are used, such as overexpression or knockdown of TJ proteins that can be achieved in *in vitro* models using cell cultures, while functional studies *in vivo* are usually performed in knockout (KO) animal models.

A. Cell Culture Models: Overexpression and Knockdown

Characterization of a TJ protein can be readily achieved by its overexpression in cell lines that show no or only weak endogenous expression of this protein. Conversely, knockdowns may be performed in cell lines showing

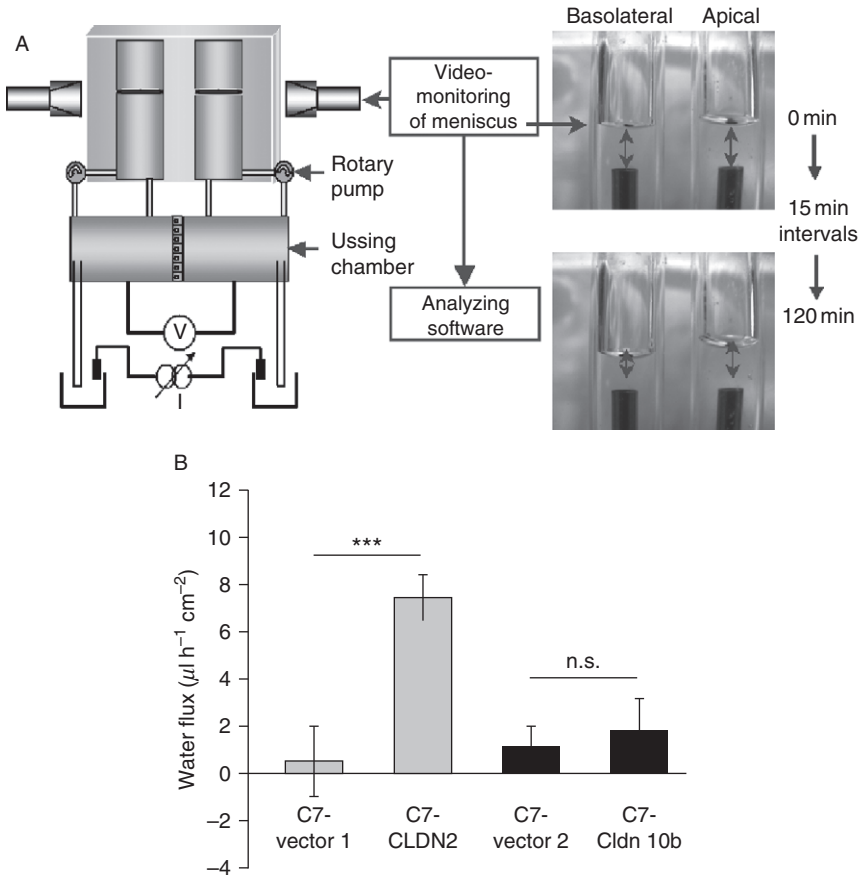

FIGURE 8 Water flux measurements in MDCK C7 cells: (A) The experimental setup consists of a modified Ussing chamber in combination with a video-optic system for monitoring the menisci in the glass tubes connected with the Ussing chamber for a period of 2 h. (B) Water flux was measured in MDCK C7 cells transfected with the cation-permeable claudins claudin-2 C7-CLDN2) or claudin-10b (C7-cldn10b) and the corresponding vector controls (C7-vector 1, 2). Water flux was stimulated by a NaCl gradient (80 mM) with the high NaCl concentration in the basolateral compartment and osmotic compensation at the apical side ($n = 7–9$). Water flux was increased in C7-CLDN2 cells in comparison to the vector control, whereas no effect could be observed in C7-cldn10b cells. Thus, only claudin-2 forms a water-permeable channel in the TJ of epithelial cells. Part (B) adapted from Rosenthal et al. (2010).

strong endogenous expression of the protein of interest. For overexpression, cDNA of the protein is cloned into an expression vector, while for knock-down, specific short-hairpin RNA (shRNA), which activates the RNA

interference system (for reviews, see Almeida & Allshire, 2005; Ouellet, Perron, Plante, & Provost, 2006), is introduced into the expression vector. As transient transfection is only affecting a fraction of cells and therefore is not suitable for a detailed and complete analysis of the protein's function, stable transfections are performed, keeping the transfected cells under antibiotic selective pressure.

Two different expression models are generally used for characterization. In constitutive expression models, the created clones are permanently affected by the transgenic expression or knockdown. Although this is a convenient method to create clones of interest, the expression pattern of other proteins may strongly differ due to the artificial environment and its influences created by the overexpression or absence of the target protein. Therefore, clones have to be screened not only for being positive for the protein of interest but also for being unchanged in all other relevant parameters. As it is impossible to analyze the whole proteome, characterization should be performed on several clones in parallel. A further complication may be the induction of lethality due to absence or high overexpression of the protein of interest which, obviously, would prevent the generation of useful clone.

Alternatively, conditional or inducible system can be used. The most widely used externally regulatable transgenic system is based on tetracycline-controlled transcriptional regulation (Gossen & Bujard, 1992; Gossen et al., 1995) and is differentiated in two basic variants, the tetracycline-controlled transcriptional activator system (tTA system; "Tet-Off") and the reverse tetracycline-controlled transcriptional activator system (rtTA system; "Tet-On").

In the "Tet-Off" system, doxycycline (Dox) is used to switch off transcription. It allows high levels of induction when in the "On" state and is comparable to the constitutive system because permanent transcription occurs in the absence of Dox. A major drawback is that this system may also lead to strong changes in endogenous protein expression and regulation.

The "Tet-On" system permits rapid activation in some systems within hours and usually no change in the endogenous expression patterns of other proteins, unless due to the transfection itself, because here Dox is used to start transcription. A disadvantage of this system is its "leakiness," that is, a permanent basal level of transgenic expression, possibly due to weak binding affinities.

B. In Vivo Models: Knockout Mice

Although cell cultures as *in vitro* models provide functional information on TJ proteins, their usefulness is limited as they cannot mimic the conditions of a complete tissue or whole organ. As endogenous TJ protein expression may

affect the TJ protein of interest, the resulting interactions and TJ changes may differ from one cell culture model to another. Similarly, the barrier properties of TJs and their components vary among different types of epi- and endothelia depending on their physiological function. This makes *in vivo* models for TJ protein and barrier characterization indispensable.

A well-established model is the KO mouse (Gordon, Scangos, Plotkin, Barbosa, & Ruddle, 1980). Here, similar to the described cell culture models, constitutive and conditional mice models are used because constitutive KOs alone may lead to lethality if expression of the target gene is important during embryonic development or if the KO results in disorders that cause early death of the offspring.

KO mice are generated using different methods and constructs, which in conditional KO, may allow time- and tissue-specific analysis of the protein of interest. Here, differently activated ligands for the regulation of gene expression are used (Cre *loxP* system; Feil, Wagner, Metzger, & Chambon, 1997; Gu, Marth, Orban, Mossmann, & Rajewsky, 1994; Metzger & Chambon, 2001).

C. Established Mouse Models

Several knockout/knockdown mouse models already exist that directly or indirectly affect the TJ. The lack of some TJ-related proteins, such as ZO-3 or claudin-6, causes no apparent phenotype in mice (Anderson et al., 2008; Hunziker, Kiener, & Xu, 2009), whereas the lack of others, such as ZO-1 and ZO-2, causes embryonic lethality (Katsuno et al., 2008; Xu et al., 2008). In contrast, knockout/knockdown animals for other TJ proteins show a distinct phenotype but are viable and may therefore be accessible to investigations with biophysical techniques. Proteins targeted in these mouse models comprise occludin, claudin-1, -5, -7, -11, -14, -16, -19, and E-cadherin.

Thorough biophysical investigations have not yet been carried out on claudin-5-, claudin-7-, claudin-11-, and claudin-14-deficient mice. Claudin-5 knockout is neonatally lethal due to blood–brain barrier loss, impressively shown by tracer movement into the brain of $Cldn5^{-/-}$ mice (Nitta et al., 2003). Claudin-$7^{-/-}$ mice show a clear growth retardation, renal salt wasting, and chronic dehydration (Tatum et al., 2010). Deficiency in claudin-11 and/or claudin-14 causes deafness, as both proteins are involved in the maintenance of inner ear epithelial barrier function (Ben-Yosef et al., 2003; Elkouby-Naor, Abassi, Lagziel, Gow, & Ben-Yosef, 2008; Gow et al., 2004). In addition, male $Cldn11^{-/-}$ mice are sterile due to an arrest of spermatogenesis caused by the lack of claudin-11 in the Sertoli cells of the testis (Gow et al., 1999; Mazaud-Guittot et al., 2010).

1. Example: Occludin

Although it was the first TJ protein discovered (Furuse et al., 1993), for a long time little was known about the function of occludin. Introduction of occludin into cells normally lacking TJs did not generate a typical anastomosing network (Furuse et al., 1996), and the disruption of both occludin alleles in embryonic stem cells resulted in polarized epithelial cells, which also formed an effective barrier to the diffusion of a low-molecular-weight tracer. Moreover, freeze-fracture replicas of these cells displayed well-developed TJ networks (Saitou et al., 1998), indicating that occludin is not required for the formation of TJ strands.

Occludin-deficient mice ($Occl^{-/-}$) displayed an extensive phenotype indicating more complex functions of occludin (Saitou et al., 2000). $Occl^{-/-}$ mice showed postnatal growth retardation, males produced no litter, while females did not suckle their litter. Calcification of the brain, testicular atrophy, thinning of compact bone, and loss of cytoplasmatic granules in striated duct cells of the salivary gland were observed together with chronic inflammation and hyperplasia in the gastric epithelium. Interestingly, no epithelial barrier defects were shown.

Further detailed analysis of the small and large intestine in comparison with stomach epithelia (Schulzke et al., 2005) unveiled a decrease in electrogenic chloride secretion in the small intestine. 1PI spectroscopy measurements showed no change in epithelial or subepithelial resistances, and the performance of conductance scanning disclosed no differences in crypt or surface epithelium of the intestine. Additional examination of the urinary bladder as a very tight epithelium showed no change after occludin knockout. Performance of mannitol flux measurements also showed no difference between wild-type and knockout mice.

In the stomach, acid secretion was found to be almost abolished. This was accompanied by a dramatic change in gastric morphology with mucus cell hyperplasia and a loss of parietal cells (Saitou et al., 2000). Those findings, once again, indicated no essential role for occludin within the TJ itself, but involvement in regulatory pathways during the differentiation of the gastric epithelium.

Another study, using a knockdown of occludin in MDCK II cells by siRNA, later revealed a role of occludin in the transduction of signals of apoptotic cells through the TJ to the actin cytoskeleton via the Rho signaling pathway (Yu et al., 2005).

2. Example: Claudin-1 and E-Cadherin

E-cadherin is an adherens junction rather than a TJ protein; however, its loss causes a redistribution of claudins within the epidermis and therefore similar barrier defects as those observed in claudin-1-deficient mice (Tunggal et al.,

2005). Both claudin-1- and E-cadherin-deficient mice die from water loss across their skin within a few hours after birth. Tracer flux experiments in claudin-1- and E-cadherin-deficient mice emphasized the impairment of epidermal barrier (Furuse et al., 2002; Tunggal et al., 2005). Furthermore, 1PI spectroscopical measurements showed that this barrier loss resulted in a dramatic decrease in R^{epi} in the skin of these mice from more than 4000 Ω cm^2 to less than 1500 Ω cm^2, whereas subepithelial resistance was unaffected (Tunggal et al., 2005).

3. Example: Claudin-15

Effects of claudin-15 loss were investigated by Tamura et al. (2008) in Cldn15$^{-/-}$ mice. A major phenotype in these mice was the development of a mega-intestine, the small intestine in Cldn15$^{-/-}$ mice being twice as long and twice in diameter compared to that of Cldn15$^{+/+}$ mice. Permeability studies disclosed no differences in the permeability of several electrically uncharged tracers between about 0.4 and 20 kDa in molecular weight. In contrast, paracellular ion permeability in the distal part of jejunum was decreased, indicating that claudin-15 specifically acts as a paracellular ion channel.

4. Example: Claudin-16

Patients with defective claudin-16 suffer from familial hypomagnesemia, hypercalciuria, and nephrocalcinosis (FHHNC). Similar symptoms were observed in claudin-16 knockdown mice generated by Hou et al. (2007) through an siRNA approach. Isolated perfused TAL tubules from these mice were used to measure R^t and to carry out ion permeability measurements. To this end, tubules are held and perfused by a concentric glass pipette system developed by Greger (1981) (see Fig. 9). The double-barreled perfusion pipette is used for voltage measurement and constant current injection so that, similar to Ussing chamber experiments, equivalent I_{SC} values can be determined. However, due to the geometry of the tubules, cable equations have to be used to calculate R^t (Greger, 1981), to allow for voltage attenuation along the tubule.

Using this technique, Hou et al. (2007) were able to demonstrate that R^t, length constant, and the transepithelial potential component due to active transport were unchanged. However, in the presence of a NaCl gradient across the epithelium, the resulting dilution potential differed greatly, indicating a reduction in P_{Na}/P_{Cl} from 3.1 to 1.5. In the intact kidney, this would cause a reduction in driving force for the reuptake of divalent cations and thus explain the observed hypomagnesemia and hypercalciuria.

5. Example: Claudin-19

Claudin-19-deficient mice were first generated by Miyamoto et al. (2005). These mice were described to present behavioral abnormalities due to Schwann cell barrier defects that affected the nerve conduction of peripheral

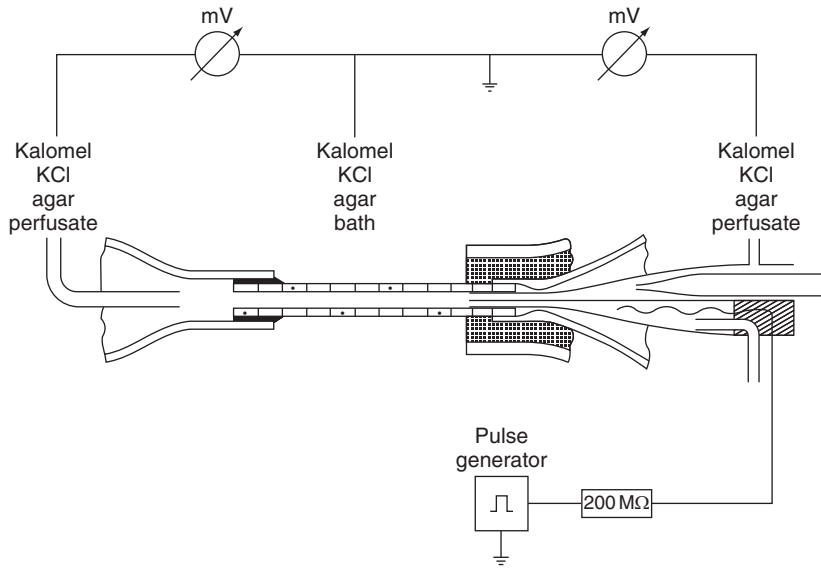

FIGURE 9 Electrophysiology on isolated kidney tubules. The tubule is constantly perfused from right to left through the upper channel of the dual-channel perfusion pipette (right). The lower channel is connected to a pulse generator via Ag-wire for the injection of current pulses. Extratubular bath solution and perfusate (right and left) are in electric contact with agar bridges which connect to calomel electrodes via 3 M KCl solution. The potential difference between these electrodes is measured with two millivoltmeters. From Greger (1981).

myelinated fibers. Recently, Hou et al. (2009) generated a cldn19-siRNA knockdown mouse. In contrast to Miyamoto et al. (2005), they found that claudin-19 knockdown affected claudin-16 distribution in the TJ of the thick ascending limb and, through this mechanism, decreased the cation permeability of these TJs. Conversely, in the absence of claudin-16, claudin-19 failed to assemble in TAL TJ, indicating that both claudins are needed for an intact barrier function of this nephron segment.

VIII. CONCLUSION

During the past 15 years, the discovery of the claudin protein family has revolutionized our understanding of epithelial function. The rapid gain in functional understanding is largely due to the fact that from the very beginning, investigations combined molecular biologic and biophysical techniques. Perturbations of TJs in various cell culture systems, tissues, and

whole organisms were achieved by the specific overexpression or downregulation of protein expression, or by treatment with different TJ-influencing agents. The resulting changes in TJ function were then characterized by a multitude of techniques, of which the present review can only give a brief comprehension and summary.

For instance, methods such as impedance spectroscopy allow to quantify changes in paracellular resistance and to separate these changes from those occurring in trans- or subcellular resistance and are thus highly superior to conventional TER measurements which at best give a rough estimate of the combined effects. In an alternative approach, paracellular permeabilities can be determined by flux or diffusion potential measurements. Here, however, it should be kept in mind that there is not THE permeability of a specimen but that there are different permeabilities for every ion or uncharged molecule of different sizes (including water), and that these permeabilities may change independently. Consequently, a closer look into the permeabilities of a broad range of solutes gives information about paracellular pore properties such as pore size, charge preferences in ion passage, and even allows the identification of independent passage pathways.

Taken together, numerous biophysical methods give the opportunity to analyze the TJ and its components under manifold aspects, and complement each other to a detailed view of paracellular pathways regulated by the TJ.

References

Agre, P., Preston, G. M., Smith, B. L., Jung, J. S., Raina, S., Moon, C., et al. (1993). Aquaporin CHIP: The archetypal molecular water channel. *American Journal of Physiology, 265*, 463–476.

Almeida, R., & Allshire, R. C. (2005). RNA silencing and genome regulation. *Trends in Cell Biology, 15*, 251–258.

Amasheh, S., Meiri, N., Gitter, A. H., Schöneberg, T., Mankertz, J., Schulzke, J. D., et al. (2002). Claudin-2 expression induces cation-selective channels in tight junctions of epithelial cells. *Journal of Cell Science, 115*, 4969–4976.

Amasheh, S., Milatz, S., Krug, S. M., Bergs, M., Amasheh, M., Schulzke, J. D., et al. (2009). Na^+ absorption defends from paracellular back-leakage by claudin-8 upregulation. *Biochemical and Biophysical Research Communications, 378*, 45–50.

Amasheh, S., Schmidt, T., Mahn, M., Florian, P., Mankertz, J., Tavalali, S., et al. (2005). Contribution of claudin-5 to barrier properties in tight junctions of epithelial cells. *Cell and Tissue Research, 321*, 89–96.

Ammann, D. (1986). *Ion-selective microelectrode and application.* Berlin: Springer Verlag.

Anderson, W. J., Zhou, Q., Alcalde, V., Kaneko, O. F., Blank, L. J., Sherwood, R. I., et al. (2008). Genetic targeting of the endoderm with claudin-6CreER. *Developmental Dynamics, 237*, 504–512.

Angelow, S., Kim, K. J., & Yu, A. S. (2006). Claudin-8 modulates paracellular permeability to acidic and basic ions in MDCK II cells. *The Journal of Physiology, 571*, 15–26.

Artursson, P., Ungell, A. L., & Lofroth, J. E. (1993). Selective paracellular permeability in two models of intestinal absorption: Cultured monolayers of human intestinal epithelial cells and rat intestinal segments. *Pharmaceutical Research, 10*, 1123–1129.

Balasubramanian, S., Lynch, J. W., & Barry, P. H. (1997). Concentration dependence of sodium permeation and sodium ion interactions in the cyclic AMP-gated channels of mammalian olfactory receptor neurons. *The Journal of Membrane Biology, 159*, 41–52.

Barry, P. H. (2006). The reliability of relative anion–cation permeabilities deduced from reversal (dilution) potential measurements in ion channel studies. *Cell Biochemistry and Biophysics, 46*, 143–154.

Barry, P. H., & Diamond, J. M. (1970). Junction potentials, electrode standard potentials, and other problems in interpreting electrical properties of membranes. *The Journal of Membrane Biology, 3*, 93–122.

Barry, P. H., & Lynch, J. W. (1991). Liquid junction potentials and small cell effects in patch-clamp analysis. *The Journal of Membrane Biology, 121*, 101–117.

Ben-Yosef, T., Belyantseva, I. A., Saunders, T. L., Hughes, E. D., Kawamoto, K., Van Itallie, C. M., et al. (2003). Claudin 14 knockout mice, a model for autosomal recessive deafness DFNB29, are deaf due to cochlear hair cell degeneration. *Human Molecular Genetics, 12*, 2049–2061.

Bijvelds, M., Kolar, Z., Bonga, S., & Flik, G. (1997). Mg^{2+} transport in plasma membrane vesicles of renal epithelium of the Mozambique tilapia (*Oreochromis mossambicus*). *The Journal of Experimental Biology, 200*, 1931–1939.

Bijvelds, M. J. C., Kolar, Z. I., Wendelaar-Bonga, S. E., & Flik, G. (1996). Magnesium transport across the basolateral plasma membrane of the fish enterocyte. *The Journal of Membrane Biology, 154*, 217–222.

Bojarski, C., Gitter, A. H., Bendfeldt, K., Mankertz, J., Schmitz, H., Wagner, S., et al. (2001). Permeability of HT-29/B6 colonic epithelium as a function of apoptosis. *The Journal of Physiology, 535*, 541–552.

Brown, D. R., & O'Grady, S. M. (2008). The Ussing chamber and measurement of drug actions on mucosal ion transport. *Current Protocols in Pharmacology, 41*, 7121–71217.

Bürgel, N., Bojarski, C., Mankertz, J., Zeitz, M., Fromm, M., & Schulzke, J. D. (2002). Mechanisms of diarrhea in collagenous colitis. *Gastroenterology, 123*, 433–443.

Carpi-Medina, P., & Whittembury, G. (1988). Comparison of transcellular and transepithelial water osmotic permeabilities (Pos) in the isolated proximal straight tubule (PST) of the rabbit kidney. *Pflügers Archiv., 412*, 66–74.

Cereijido, M., Stefani, E., & Palomo, A. M. (1980). Occluding junctions in a cultured transporting epithelium: Structural and functional heterogeneity. *The Journal of Membrane Biology, 53*, 19–32.

Clarke, L. L. (2009). A guide to Ussing chamber studies of mouse intestine. *American Journal of Physiology. Gastrointestinal and Liver Physiology, 296*, G1151–G1166.

Claude, P. (1978). Morphological factors influencing transepithelial permeability: A model for the resistance of the zonula occludens. *The Journal of Membrane Biology, 39*, 219–232.

Claude, P., & Goodenough, D. A. (1973). Fracture faces of zonulae occludentes from "tight" and "leaky" epithelia. *The Journal of Cell Biology, 58*, 390–400.

Clausen, C., Lewis, S. A., & Diamond, J. M. (1979). Impedance analysis of a tight epithelium using a distributed resistance model. *Biophysical Journal, 26*, 291–318.

Cole, K. S., & Curtis, H. J. (1938a). Electrical impedance of nerve during activity. *Nature, 142*, 209–210.

Cole, K. S., & Curtis, H. J. (1938b). Electrical impedance of Nitella during activity. *The Journal of General Physiology, 21*, 37–64.

Cole, K. S., & Curtis, H. J. (1938c). Electrical impedance of single marine eggs. *The Journal of General Physiology, 21*, 591–599.

Curtis, H. J., & Cole, K. S. (1938). Transverse electric impedance of the squid giant axon. *The Journal of General Physiology, 21*, 757–765.

Dwyer, T. M., Adams, D. J., & Hille, B. (1980). The permeability of the endplate channel to organic cations in frog muscle. *The Journal of General Physiology, 75*, 469–492.

Eisenman, G. (1962). Cation selective glass electrodes and their mode of operation. *Biophysical Journal, 2*, 259–323.

Elkouby-Naor, L., Abassi, Z., Lagziel, A., Gow, A., & Ben-Yosef, T. (2008). Double gene deletion reveals lack of cooperation between claudin 11 and claudin 14 tight junction proteins. *Cell and Tissue Research, 333*, 427–438.

Farquhar, M. G., & Palade, G. E. (1963). Junctional complexes in various epithelia. *The Journal of Cell Biology, 17*, 375–412.

Feil, R., Wagner, J., Metzger, D., & Chambon, P. (1997). Regulation of Cre recombinase activity by mutated estrogen receptor ligand-binding domains. *Biochemical and Biophysical Research Communications, 237*, 752–757.

Flamion, B., Spring, K. R., & Abramow, M. (1995). Adaptation of inner medullary collecting duct to dehydration involves a paracellular pathway. *American Journal of Physiology, 268*, 53–63.

Florian, P., Schöneberg, T., Schulzke, J. D., Fromm, M., & Gitter, A. H. (2002). Single-cell epithelial defects close rapidly by an actinomyosin purse string mechanism with functional tight junctions. *The Journal of Physiology, 545*, 485–499.

Foskett, J. K., & Scheffey, C. (1989). Scanning electrode localization of transport pathways in epithelial tissues. *Methods in Enzymology, 171*, 792–813.

Fricke, H. (1925). The electric capacity of suspensions of red corpuscles of a dog. *Physical Review, 26*, 682–687.

Fromm, M., Krug, S. M., Zeissig, S., Richter, J. F., Rosenthal, R., Schulzke, J. D., et al. (2009). High resolution analysis of barrier function. *Annals of the New York Academy of Sciences, 1165*, 74–81.

Frömter, E. (1972). The route of passive ion movement through the epithelium of Necturus gallbladder. *The Journal of Membrane Biology, 8*, 259–301.

Frömter, E., & Diamond, J. (1972). Route of passive ion permeation in epithelia. *Nature: New Biology, 235*, 9–13.

Furuse, M., Fujimoto, K., Sato, N., Hirase, T., Tsukita, S., & Tsukita, S. (1996). Overexpression of occludin, a tight junction-associated integral membrane protein, induces the formation of intracellular multilamellar bodies bearing tight junction-like structures. *Journal of Cell Science, 109*, 429–435.

Furuse, M., Furuse, K., Sasaki, H., & Tsukita, S. (2001). Conversion of zonulae occludentes from tight to leaky strand type by introducing claudin-2 into Madin-Darby canine kidney I cells. *The Journal of Cell Biology, 153*, 263–272.

Furuse, M., Hata, M., Furuse, K., Yoshida, Y., Haratake, A., Sugitani, Y., et al. (2002). Claudin-based tight junctions are crucial for the mammalian epidermal barrier: A lesson from claudin-1-deficient mice. *The Journal of Cell Biology, 156*, 1099–1111.

Furuse, M., Hirase, T., Itoh, M., Nagafuchi, A., Yonemura, S., Tsukita, S., et al. (1993). Occludin: A novel integral membrane protein localizing at tight junctions. *The Journal of Cell Biology, 123*, 1777–1788.

Ghandehari, H., Smith, P. L., Ellens, H., Yeh, P. Y., & Kopecek, J. (1997). Size-dependent permeability of hydrophilic probes across rabbit colonic epithelium. *The Journal of Pharmacology and Experimental Therapeutics, 280*, 747–753.

Gitter, A. H., Bendfeldt, K., Schulzke, J. D., & Fromm, M. (2000a). Leaks in the epithelial barrier caused by spontaneous and TNFa-induced single-cell apoptosis. *FASEB Journal, 14*, 1749–1753.

Gitter, A. H., Bendfeldt, K., Schulzke, J. D., & Fromm, M. (2000b). Trans-/paracellular, surface/crypt, and epithelial/subepithelial resistances of mammalian colonic epithelia. *Pflügers Archiv, 439*, 477–482.

Gitter, A. H., Bertog, M., Schulzke, J. D., & Fromm, M. (1997). Measurement of paracellular epithelial conductivity by conductance scanning. *Pflügers Archiv, 434*, 830–840.

Gitter, A. H., Wullstein, F., Fromm, M., & Schulzke, J. D. (2001). Epithelial barrier defects in ulcerative colitis: Characterization and quantification by electrophysiological imaging. *Gastroenterology, 121*, 1320–1328.

Gordon, J. W., Scangos, G. A., Plotkin, D. J., Barbosa, J. A., & Ruddle, F. H. (1980). Genetic transformation of mouse embryos by microinjection of purified DNA. *Proceedings of the National Academy of Sciences of the United States of America, 77*, 7380–7384.

Gossen, M., & Bujard, H. (1992). Tight control of gene expression in mammalian cells by tetracycline-responsive promoters. *Proceedings of the National Academy of Sciences of the United States of America, 89*, 5547–5551.

Gossen, M., Freundlieb, S., Bender, G., Muller, G., Hillen, W., & Bujard, H. (1995). Transcriptional activation by tetracyclines in mammalian cells. *Science, 268*, 1766–1769.

Goulding, E. H., Tibbs, G. R., Liu, D., & Siegelbaum, S. A. (1993). Role of H5 domain in determining pore diameter and ion permeation through cyclic nucleotide-gated channels. *Nature, 364*, 61–64.

Gow, A., Davies, C., Southwood, C. M., Frolenkov, G., Chrustowski, M., Ng, L., et al. (2004). Deafness in Claudin 11-null mice reveals the critical contribution of basal cell tight junctions to stria vascularis function. *The Journal of Neuroscience, 24*, 7051–7062.

Gow, A., Southwood, C. M., Li, J. S., Pariali, M., Riordan, G. P., Brodie, S. E., et al. (1999). CNS myelin and sertoli cell tight junction strands are absent in Osp/claudin-11 null mice. *Cell, 99*, 649–659.

Greger, R. (1981). Cation selectivity of the isolated perfused cortical thick ascending limb of Henle's loop of rabbit kidney. *Pflügers Archiv, 390*, 30–37.

Grotjohann, I., Gitter, A. H., Köckerling, A., Bertog, M., Schulzke, J. D., & Fromm, M. (1998). Localization of cAMP- and aldosterone-induced K^+ secretion in rat distal colon by conductance scanning. *The Journal of Physiology, 507*, 561–570.

Gu, H., Marth, J. D., Orban, P. C., Mossmann, H., & Rajewsky, K. (1994). Deletion of a DNA polymerase beta gene segment in T cells using cell type-specific gene targeting. *Science, 265*, 103–106.

Günzel, D., Amasheh, S., Pfaffenbach, S., Richter, J. F., Kausalya, P. J., Hunziker, W., et al. (2009). Claudin-16 affects transcellular Cl^- secretion in MDCK cells. *The Journal of Physiology (London), 587*, 3777–3793.

Günzel, D., Florian, P., Richter, J. F., Troeger, H., Schulzke, J. D., Fromm, M., et al. (2006). Restitution of single-cell defects in the mouse colon epithelium differs from that of cultured cells. *American Journal of Physiology. Regulatory, Integrative and Comparative Physiology, 290*, R1496–R1507.

Günzel, D., Stuiver, M., Kausalya, P. J., Haisch, L., Krug, S. M., Rosenthal, R., et al. (2009). Claudin-10 exists in six alternatively spliced isoforms which exhibit distinct localization and function. *Journal of Cell Science, 122*, 1507–1517.

Günzel, D., & Yu, A. S. L. (2009). Function and regulation of claudins in the thick ascending limb of Henle. *Pflügers Archiv, 458*, 77–88.

Hernandez, C. S., Gonzalez, E., & Whittembury, G. (1995). The paracellular channel for water secretion in the upper segment of the Malpighian tubule of *Rhodnius prolixus*. *The Journal of Membrane Biology, 148*, 233–242.

Höber, R. (1910). Eine Methode, die elektrische Leitfähigkeit im Innern von Zellen zu messen. *Pflügers Archiv, 133*, 237–253.

Hou, J., Paul, D. L., & Goodenough, D. A. (2005). Paracellin-1 and the modulation of ion selectivity of tight junctions. *Journal of Cell Science, 118*, 5109–5118.

Hou, J., Renigunta, A., Gomes, A. S., Hou, M., Paul, D. L., Waldegger, S., et al. (2009). Claudin-16 and claudin-19 interaction is required for their assembly into tight junctions and for renal reabsorption of magnesium. *Proceedings of the National Academy of Sciences of the United States of America, 106*, 15350–15355.

Hou, J., Shan, Q., Wang, T., Gomes, A. S., Yan, Q., Paul, D. L., et al. (2007). Transgenic RNAi depletion of claudin-16 and the renal handling of magnesium. *The Journal of Biological Chemistry, 282*, 17114–17122.

Hudspeth, A. J. (1975). Establishment of tight junctions between epithelial cells. *Proceedings of the National Academy of Sciences of the United States of America, 72*, 2711–2713.

Hunziker, W., Kiener, T. K., & Xu, J. (2009). Vertebrate animal models unravel physiological roles for zonula occludens tight junction adaptor proteins. *Annals of the New York Academy of Sciences, 1165*, 28–33.

Ikari, A., Hirai, N., Shiroma, M., Harada, H., Sakai, H., Hayashi, H., et al. (2004). Association of paracellin-1 with ZO-1 augments the reabsorption of divalent cations in renal epithelial cells. *The Journal of Biological Chemistry, 279*, 54826–54832.

Ikenouchi, J., Furuse, M., Furuse, K., Sasaki, H., Tsukita, S., & Tsukita, S. (2005). Tricellulin constitutes a novel barrier at tricellular contacts of epithelial cells. *The Journal of Cell Biology, 171*, 939–945.

Jaffe, L. F., & Nuccitelli, R. (1974). An ultrasensitive vibrating probe for measuring steady extracellular currents. *The Journal of Cell Biology, 63*, 614–628.

Jovov, B., Wills, N. K., & Lewis, S. A. (1991). A spectroscopic method for assessing confluence of epithelial cell cultures. *American Journal of Physiology, 261*, C1196–C1203.

Katsuno, T., Umeda, K., Matsui, T., Hata, M., Tamura, A., Itoh, M., et al. (2008). Deficiency of ZO-1 causes embryonic lethal phenotype associated with defected yolk sac angiogenesis and apoptosis of embryonic cells. *Molecular Biology of the Cell, 19*, 2465–2475.

Kausalya, P. J., Amasheh, S., Günzel, D., Wurps, H., Müller, D., Fromm, M., et al. (2006). Disease-associated mutations affect intracellular traffic and paracellular Mg^{2+} transport function of claudin-16. *The Journal of Clinical Investigation, 116*, 878–891.

Knepper, M. A. (1994). The aquaporin family of molecular water channels. *Proceedings of the National Academy of Sciences of the United States of America, 91*, 6255–6258.

Knipp, G. T., Ho, N. F., Barsuhn, C. L., & Borchardt, R. T. (1997). Paracellular diffusion in Caco-2 cell monolayers: Effect of perturbation on the transport of hydrophilic compounds that vary in charge and size. *Journal of Pharmaceutical Sciences, 86*, 1105–1110.

Köckerling, A., & Fromm, M. (1993). Origin of cAMP-dependent Cl^- secretion from both crypts and surface epithelia of rat intestine. *American Journal of Physiology, 264*, C1294–C1301.

Köckerling, A., Sorgenfrei, D., & Fromm, M. (1993). Electrogenic Na^+ absorption of rat distal colon is confined to surface epithelium. A voltage scanning study. *The American Journal of Physiology, 264*, C1285–C1293.

Kottra, G., & Frömter, E. (1984). Rapid determination of intraepithelial resistance barriers by alternating current spectroscopy: Experimental procedures. *Pflügers Archiv, 402*, 409–420.

Kovbasnjuk, O., Leader, J. P., Weinstein, A. M., & Spring, K. R. (1998). Water does not flow across the tight junctions of MDCK cell epithelium. *Proceedings of the National Academy of Sciences of the United States of America, 95*, 6526–6530.

Kroesen, A. J., Dullat, S., Schulzke, J. D., Fromm, M., & Buhr, H. J. (2008). Permanently increased mucosal permeability in patients with backwashileitis after ileoanal pouch for ulcerative colitis. *Scandinavian Journal of Gastroenterology, 43*, 704–711.

Krug, S. M., Amasheh, S., Richter, J. F., Milatz, S., Günzel, D., Westphal, J. K., et al. (2009). Tricellulin forms a barrier to macromolecules in tricellular tight junctions without affecting ion permeability. *Molecular Biology of the Cell, 20*, 3713–3724.

Krug, S. M., Fromm, M., & Günzel, D. (2009). Two-path impedance spectroscopy for measurement of paracellular and transcellular epithelial resistance. *Biophysical Journal, 97*, 2202–2211.

Lewis, S. A., Eaton, D. C., Clausen, C., & Diamond, J. M. (1977). Nystatin as a probe for investigating the electrical properties of a tight epithelium. *The Journal of General Physiology, 70*, 427–440.

Madara, J. L., & Dharmsathaphorn, K. (1985). Occluding junction structure-function relationships in a cultured epithelial monolayer. *The Journal of Cell Biology, 101*, 2124–2133.

Mankertz, J., Amasheh, M., Krug, S. M., Fromm, A., Hillenbrand, B., Tavalali, S., et al. (2009). Tumour necrosis factor alpha up-regulates claudin-2 expression in epithelial HT-29/B6 cells via phosphatidylinositol 3-kinase signaling. *Cell and Tissue Research, 336*, 67–77.

Martinez-Palomo, A., Meza, I., Beaty, G., & Cereijido, M. (1980). Experimental modulation of occluding junctions in a cultured transporting epithelium. *The Journal of Cell Biology, 87*, 736–745.

Mazaud-Guittot, S., Meugnier, E., Pesenti, S., Wu, X., Vidal, H., Gow, A., et al. (2010). Claudin 11 deficiency in mice results in loss of the Sertoli cell epithelial phenotype in the testis. *Biology of Reproduction, 82*, 202–213.

McClendon, J. F. (1927). Colloid properties of the surface of the living cell: III. Electrical impedance and reactance of blood and muscle to alternating currents of 0–1, 500, 000 cycles per second. *American Journal of Physiology, 82*, 525–532.

McClendon, J. F. (1936). Electric impedance and permeability of living cells. *Science, 84*, 184–185.

Meier, P. C., Ammann, D., Morf, W. E., & Simon, W. (1980). Liquid-membrane ion-selective electrodes and their biomedical applications. In J. Koryta (Ed.), *Medical and biological applications of electrochemical applications of electrochemical devices* (p. 13). New York: Wiley.

Metzger, D., & Chambon, P. (2001). Site- and time-specific gene targeting in the mouse. *Methods, 24*, 71–80.

Miyamoto, T., Morita, K., Takemoto, D., Takeuchi, K., Kitano, Y., Miyakawa, T., et al. (2005). Tight junctions in Schwann cells of peripheral myelinated axons: A lesson from claudin-19-deficient mice. *The Journal of Cell Biology, 169*, 527–538.

Morf, W. E. (1981). *The principles of ion-selective electrodes and of membrane transport.* Budapest/Elsevier, Amsterdam, New York: Akadémiai Kiadó.

Ng, B., & Barry, P. H. (1995). The measurement of ionic conductivities and mobilities of certain less common organic ions needed for junction potential corrections in electrophysiology. *Journal of Neuroscience Methods, 56*, 37–41.

Nitta, T., Hata, M., Gotoh, S., Seo, Y., Sasaki, H., Hashimoto, N., et al. (2003). Size-selective loosening of the blood-brain barrier in claudin-5-deficient mice. *The Journal of Cell Biology, 161*, 653–660.

Ouellet, D. L., Perron, M. P., Plante, P., & Provost, P. (2006). MicroRNAs in gene regulation: When the smallest governs it all. *Journal of Biomedicine and Biotechnology, 2006*, 69616.

Poler, S. M., & Reuss, L. (1987). Protamine alters apical membrane K^+ and Cl^- permeability in gallbladder epithelium. *American Journal of Physiology, 253*, 662–671.

Reiter, B., Kraft, R., Günzel, D., Zeissig, S., Schulzke, J. D., Fromm, M., et al. (2006). TRPV4-mediated regulation of epithelial permeability. *FASEB Journal, 20*, 1802–1812.

Robinson, R. A., & Stokes, R. H. (1959). *Electrolyte solutions* (2nd ed.). Mineola, NY: Dover.

Rosenthal, R., Milatz, S., Krug, S. M., Oelrich, B., Schulzke, J. D., Amasheh, S., et al. (2010). Claudin-2, a component of the tight junction, forms a paracellular water channel. *Journal of Cell Science, 123*, 1913–1921.

Saitou, M., Fujimoto, K., Doi, Y., Itoh, M., Fujimoto, T., Furuse, M., et al. (1998). Occludin-deficient embryonic stem cells can differentiate into polarized epithelial cells bearing tight junctions. *The Journal of Cell Biology, 141*, 397–408.

Saitou, M., Furuse, M., Sasaki, H., Schulzke, J. D., Fromm, M., Takano, H., et al. (2000). Complex phenotype of mice lacking occludin, a component of tight junction strands. *Molecular Biology of the Cell, 11*, 4131–4142.

Sanders, S. E., Madara, J. L., McGuirk, D. K., Gelman, D. S., & Colgan, S. P. (1995). Assessment of inflammatory events in epithelial permeability: A rapid screening method using fluorescein dextrans. *Epithelial Cell Biology, 4*, 25–34.

Schulzke, J. D., Gitter, A. H., Mankertz, J., Spiegel, S., Seidler, U., Amasheh, S., et al. (2005). Epithelial transport and barrier function in occludin-deficient mice. *Biochimica et Biophysica Acta, 1669*, 34–42.

Segawa, A., Yamashina, S., & Murakami, M. (2002). Visualization of 'water secretion' by confocal microscopy in rat salivary glands: Possible distinction of para- and transcellular pathway. *European Journal of Morphology, 40*, 241–246.

Shachar-Hill, B., & Hill, A. E. (1993). Convective fluid flow through the paracellular system of Necturus gall-bladder epithelium as revealed by dextran probes. *The Journal of Physiology, 468*, 463–486.

Simon, D. B., Lu, Y., Choate, K. A., Velazquez, H., Al-Sabban, E., Praga, M., et al. (1999). Paracellin-1, a renal tight junction protein required for paracellular Mg^{2+} resorption. *Science, 285*, 103–106.

Spring, K. R. (1998). Routes and mechanism of fluid transport by epithelia. *Annual Review of Physiology, 60*, 105–119.

Steward, M. C. (1982). Paracellular non-electrolyte permeation during fluid transport across rabbit gall-bladder epithelium. *The Journal of Physiology, 322*, 419–439.

Sugiharto, S., Lewis, T. M., Moorhouse, A. J., Schofield, P. R., & Barry, P. H. (2008). Anion-cation permeability correlates with hydrated counterion size in glycine receptor channels. *Biophysical Journal, 95*, 4698–4715.

Tamura, A., Kitano, Y., Hata, M., Katsuno, T., Moriwaki, K., Sasaki, H., et al. (2008). Megaintestine in claudin-15-deficient mice. *Gastroenterology, 134*, 523–534.

Tang, V. W., & Goodenough, D. A. (2003). Paracellular Ion Channel at the Tight Junction. *Biophysical Journal, 84*, 1660–1673.

Tatum, R., Zhang, Y., Salleng, K., Lu, Z., Lin, J. J., Lu, Q., et al. (2010). Renal salt wasting and chronic dehydration in claudin-7-deficient mice. *American Journal of Physiology. Cell Physiology, 298*, F24–F34.

Tavelin, S., Taipalensuu, J., Soderberg, L., Morrison, R., Chong, S., & Artursson, P. (2003). Prediction of the oral absorption of low-permeability drugs using small intestine-like 2/4/A1 cell monolayers. *Pharmaceutical Research, 20*, 397–405.

Teorell, T. (1946). Application of "square wave analysis" to bioelectric studies. *Acta Physiologica Scand., 12*, 235–254.

Thomas, R. C. (1978). *Ion-Sensitive Intracellular Microelectrto Make and Use Them.* London: Academic Press.

Troeger, H., Epple, H. J., Schneider, T., Wahnschaffe, U., Ullrich, R., Burchard, G. D., et al. (2007). Effect of chronic *Giardia lamblia* infection on epithelial transport and barrier function in human duodenum. *Gut, 56*, 328–335.

Tunggal, J. A., Helfrich, I., Schmitz, A., Schwarz, H., Günzel, D., Fromm, M., et al. (2005). E-cadherin is essential for in vivo epidermal barrier function by regulating tight junctions. *EMBO Journal, 24*, 1146–1156.

Ussing, H. H. (1949). The distinction by means of tracers between active transport and diffusion. *Acta Physiologica Scand., 19*, 43–56.

Van Itallie, C. M., Holmes, J., Bridges, A., Gookin, J. L., Coccaro, M. R., Proctor, W., et al. (2008). The density of small tight junction pores varies among cell types and is increased by expression of claudin-2. *Journal of Cell Science, 121*, 298–305.

Van Itallie, C., Rahner, C., & Anderson, J. M. (2001). Regulated expression of claudin-4 decreases paracellular conductance through a selective decrease in sodium permeability. *The Journal of Clinical Investigation, 107*, 1319–1327.

Van Itallie, C. M., Rogan, S., Yu, A., Vidal, L. S., Holmes, J., & Anderson, J. M. (2006). Two splice variants of claudin-10 in the kidney create paracellular pores with different ion selectivities. *American Journal of Physiology. Cell Physiology, 291*, F1288–F1299.

Watson, C. J., Rowland, M., & Warhurst, G. (2001). Functional modeling of tight junctions in intestinal cell monolayers using polyethylene glycol oligomers. *American Journal of Physiology. Cell Physiology, 281*, 388–397.

Whittembury, G., Malnic, G., Mello-Aires, M., & Amorena, C. (1988). Solvent drag of sucrose during absorption indicates paracellular water flow in the rat kidney proximal tubule. *Pflügers Archiv, 412*, 541–547.

Wills, N. K., Lewis, S. A., & Eaton, D. C. (1979). Active and passive properties of rabbit descending colon: A microelectrode and nystatin study. *The Journal of Membrane Biology, 45*, 81–108.

Xu, J., Kausalya, P. J., Phua, D. C., Ali, S. M., Hossain, Z., & Hunziker, W. (2008). Early embryonic lethality of mice lacking ZO-2, but not ZO-3, reveals critical and nonredundant roles for individual zonula occludens proteins in mammalian development. *Molecular and Cellular Biology, 28*, 1669–1678.

Yu, A. S. L., Cheng, M. H., Angelow, S., Günzel, D., Kanzawa, S. A., Schneeberger, E. E., et al. (2009). Molecular basis for cation selectivity in claudin-2-based paracellular pores: Identification of an electrostatic interaction site. *The Journal of General Physiology, 133*, 111–127.

Yu, A. S., McCarthy, K. M., Francis, S. A., McCormack, J. M., Lai, J., Rogers, R. A., et al. (2005). Knockdown of occludin expression leads to diverse phenotypic alterations in epithelial cells. *American Journal of Physiology. Cell Physiology, 288*, C1231–C1241.

Zeissig, S., Bürgel, N., Günzel, D., Richter, J. F., Mankertz, J., Wahnschaffe, U., et al. (2007). Changes in expression and distribution of claudin 2, 5 and 8 lead to discontinuous tight junctions and barrier dysfunction in active Crohn's disease. *Gut, 56*, 61–72.